1

2

3

Climate Change Impacts on Net Primary Production (NPP) and Export Production (EP) Regulated by Increasing Stratification and Phytoplankton Community Structure in the CMIP5 Models

7
8
9
10

Weiwei Fu, James T. Randerson and J. Keith Moore

12

13

14

Department of Earth System Science, University of California, Irvine, California, USA, 92697

17

18   **Abstract**

19   We examine climate change impacts on net primary production (NPP) and

20   export production (sinking particulate flux; EP) with simulations from nine Earth

21   System Models (ESMs) performed in the framework of the fifth Coupled Model

22   Inter-comparison Project (CMIP5). Global NPP and EP are reduced by the end of

23   the century for the intense warming scenario of Representative Concentration

24   Pathway (RCP) 8.5. Relative to the 1990s, NPP in the 2090s is reduced by 2-16%

25   and EP by 7-18%. The models with the largest increases in stratification (and

26   largest relative declines in NPP and EP) also show the largest positive biases in

27   stratification for the contemporary period, suggesting overestimation of climate

28   change impacts on NPP and EP. All of the CMIP5 models show an increase in

29   stratification in response to surface-ocean warming and freshening, which is

30   accompanied by decreases in surface nutrients, NPP, and EP.

31   There is considerable variability across the models in the magnitudes of NPP,

32   EP, surface nutrient concentrations, and their perturbations by climate change.

33   The negative response of NPP and EP to increasing stratification reflects

34   primarily a bottom-up control, as upward nutrient flux declines at the global

35   scale. Models with dynamic phytoplankton community structure show larger

36   declines in EP than in NPP. This pattern is driven by phytoplankton community

37   composition shifts, with reductions in productivity by large phytoplankton as

38   smaller phytoplankton (which export less efficiently) are favored under the

39   increasing nutrient stress. Thus, the projections of the NPP response to climate

40   change are critically dependent on the simulated phytoplankton community

41   structure, the efficiency of the biological pump, and the resulting levels of

42   regenerated production, which vary widely across the models. Community

43   structure is represented simply in the CMIP5 models, and should be expanded to

44	better capture the spatial patterns and climate-driven changes in export

45	efficiency.

46

1 Introduction

Ocean net primary production (NPP) and particulate organic carbon export (EP) are key elements of marine biogeochemistry that are vulnerable to ongoing climate change from rising concentrations of atmospheric CO_2 and other greenhouse gases. Ocean warming has increasing impacts on ocean ecosystems by modifying the ecophysiology and distribution of marine organisms, and by altering ocean circulation and stratification. Ocean ecosystems also are important components of the climate system, influencing the atmospheric abundance of radiative agents such as CO_2, N_2O, aerosols, and the bio-optical properties of seawater (Siegenthaler and Wenk, 1984; Goldstein et al., 2003; Manizza et al., 2008; Schmittner et al., 2008; Bopp et al., 2013). Therefore, understanding the mechanisms controlling NPP and EP is essential for understanding the global cycles of carbon and other bioactive elements, and their links to climate. (Passow and Carlson, 2012).

Upper ocean stratification plays a key role in ocean biogeochemical processes. In particular, mixed layer depth (MLD) regulates the interplay between light availability for photosynthesis (Hannon et al., 2001) and nutrient supply to the upper ocean (Pollard et al., 2009). Upper ocean stratification is defined here as the density difference between the surface and 200 m depth (Capotondi et al., 2012), which is indicative of the degree of coupling and nutrient fluxes between the euphotic zone and the ocean interior. The density gradient at the base of the mixed layer affects entrainment processes, which play a crucial role in mixed layer deepening and in particle sinking/export from the euphotic zone. Stratification can also influence ocean ventilation (Luo et al., 2009), which has important consequences for oceanic uptake of carbon and oxygen. Thus, changes

4

72   in stratification over the remainder of the 21st century have the potential to

73   influence NPP and EP across marine ecosystems.

74   Stratification tends to increase in response to ocean surface warming and

75   freshening in 21st century climate change simulations. Increased stratification

76   reduces the input of sub-surface nutrients to the euphotic zone and can lead to

77   decreasing NPP and EP through increasing nutrient limitation. Many studies

78   have suggested decreases in global NPP and EP over the 21 century using

79   models with varying degrees of complexity (Bopp et al., 2001; Plattner et al., 2001;

80   Fung et al., 2005; Schmittner et al., 2008; Steinacher et al., 2009; Dutkiewicz et al.,

81   2013; Cabré et al., 2015). For the RCP8.5 scenario, CMIP5 ESM estimates of

82   changes in export production range from −7 to −18% relative to the 1990s, and for

83   NPP these changes range from −2 to −16% (Bopp et al., 2013).

84   The relative importance of different ecological controls on NPP and EP

85   depends, in part, on an individual model's capacity to represent plankton

86   functional types (PFT) (Le Quere et al., 2005; Jin et al., 2006) and their unique

87   physiological and ecological characteristics, which determine how efficiently

88   they are exported from surface waters. Increasing nutrient stress can shift

89   phytoplankton community composition, favoring smaller phytoplankton, which

90   are more efficient at nutrient uptake, over larger phytoplankton (Bopp et al., 2001;

91   Steinacher et al., 2010; Vichi et al., 2011; Moore et al., 2013). These community

92   shifts can modify the efficiency of carbon export. However, treatment of

93   plankton communities is relatively simple in the CMIP5 models, with 1-3

94   phytoplankton functional types and typically one zooplankton group (Bopp et al.,

95   2013).

96   Several previous studies examined the biogeochemical response to climate

97   change in the CMIP5 models. Bopp et al. (2013) examined output from 10 CMIP5

98   models emphasizing model mean biogeochemical responses to multiple stressors

99   and trends over the 21st century relative to 1990s means for each model. Cabré et

100   al. (2015) analyzed the CMIP5 models examining changes between model output

101   averaged over the period 1980-1999 with years 2080-2099. This study broke down

102   the global output into different ocean biomes for analysis. Laufkötter et al. (2015)

103   also analyzed output from nine coupled climate-carbon ESMs, including many of

104   the CMIP5 models to study how climate change processes impact NPP,

105   comparing two twenty-year periods (2012-2031 and 2081-2100). They suggested

106   strong roles for temperature and top-down grazing control in driving the NPP

107   response, particularly at lower latitudes. Both Cabré et al. (2015) and Laufkötter

108   et al. (2015) conclude that changing light levels were not a primary driver of

109   changes in NPP except at the highest latitudes where there were large decreases

110   in sea ice cover. Thus, we do not consider light effects in this work, where our

111   focus is on global-scale trends. More detailed regional studies of the CMIP5

112   model output have been carried out for the Arctic Ocean (Vancoppenolle et al.,

113   2013) and the Southern Ocean (Hauck and Volker, 2015; Ito et al., 2015; Leung et

114   al., 2015).

115   We analyzed centennial-scale changes in NPP and EP in response to

116   increasing surface stratification and other physical factors. We use historical

117   (1850-2005) and Representative Concentration Pathway (RCP) 8.5 (2006-2100)

118   ESM simulations from the fifth phase of the Coupled Model Inter-comparison

119   Project (CMIP5) to study long-term trends in NPP and EP and to identify the

120   mechanisms behind these changes, including the physical factors that regulate

121   nutrient availability. We also examined variability in NPP, EP, and surface

122   nutrient concentrations across the models, to highlight some of the large

123   differences and uncertainties in projections of climate change impacts on marine

124   biogeochemistry in current-generation ESMs.

125

126   **2 Methods**

127   We analyzed simulations from a set of 9 ESMs that contributed output to the

128   Earth System Grid Federation as a part of CMIP5 (Taylor et al., 2012). Required

129   physical ocean variables were temperature, salinity, and potential density;

130   required biogeochemistry variables were macronutrients (nitrate, phosphate, and

131   silicic acid), iron, chlorophyll, NPP and EP. The selection of the 9 models

132   investigated here (Table 1) was based on the availability of these variables.

133   The historical and RCP8.5 simulations we analyzed had prescribed

134   atmospheric CO_2 mole fractions and forcing from other greenhouse gases and

135   aerosols, anthropogenic land use, and solar variability. Volcanic forcing also was

136   included during the historical period. The RCP 8.5 is a strong warming scenario

137   with an increase in radiative forcing of 8.5 W/m^2 by 2100 as atmospheric CO_2

138   mole fractions reach 936 ppm (Moss et al., 2010; van Vuuren et al., 2011). In the

139   case where several ensemble members were available from an individual ESM,

140   we analyzed only the first member.

141   A simple description of the 9 ESMs is presented in Tables 1 and 2.

142   Atmospheric and ocean resolutions vary across the models (Table 1). Typical

143   atmospheric horizontal grid resolution is ~2°, but it ranges from 0.94° to 3.8°.

144   Typical ocean horizontal resolution is ~1°, ranging from 0.3° to 2°. In the vertical,

145   there are 24 to 95 levels in the atmosphere and 31 to 63 levels in the ocean. All

146   marine biogeochemical components are nutrient–phytoplankton–zooplankton–

147   detritus (NPZD) models, but with varying degrees of complexity, illustrated for

7

148   instance by the number of phytoplankton functional groups (from 1 to 3) or

149   limiting nutrients (from 3 to 5) that are explicitly represented (Table 2).

150   In our analysis, we used the CMIP5 variable denoting the vertical integration

151   of NPP (intpp) and sinking export of organic particles at 100 m (EP; epc100). We

152   present global mean estimates as the area-weighted or volume-weighted mean

153   by the grid-cell area/volume from an individual model. Monthly mean data are

154   averaged to obtain annual means and the annual mean data are interpolated

155   onto a common 1°×1° regular grid for the comparison of the 2-D fields.

156

157   **3 Results**

158   **3.1 Stratification changes**

159   Stratification, defined here as the density difference between the depth of 200

160   m and the surface, is a useful indicator of change in the upper ocean, as it

161   integrates changes in both temperature and salinity. In Figure 1a, we present the

162   time series of global mean stratification changes for the historical period and the

163   RCP8.5 projection. All the models project an increase in stratification (ranging

164   from 6% to 30% by the 2090s). However, the amplitude of stratification differs

165   considerably across the models. The GFDL-ESM2M and MPI models are

166   relatively close to the observed mean stratification in the WOA09 dataset (red

167   square, 1.81 kg/m^3) for the present era. NorESM1-ME shows the weakest

168   stratification (1.74 kg/m^3) while the stratification in HadGEM2-ES is strongest

169   (2.45 kg/m^3). Long-term trends are in general agreement across models, but the

170   rate of stratification increase varies, with IPSL-CM5A-MR showing the most

171   rapid increase and NorESM1-ME the slowest increase.

172   Surface processes that decrease density can largely explain the stratification

173   increase in the RCP8.5 projections. Global mean sea surface temperature (SST)

8

174 warms by 2.6-3.5°C, accompanied by sea surface salinity (SSS) decreases of 0.05-

175 0.25 psu over the 21st century (Figure 1). By 2100, the global mean SST ranges

176 from 20.4°C (HadGEM2-ES) to 21.8°C (NorESM1-ME). Model spread decreases

177 in the RCP8.5 projections in response to strong anthropogenic forcing (Figure 1b).

178 SSS shows a clear declining tendency from 1850 to 2100 (Figure 1). Compared to

179 the WOA09 observational data, most of the models are too fresh at the surface in

180 the 1990s, especially the HadGEM2-ES, which has the lowest global mean SSS.

181 The model spread is partly due to internal variability simulated by the climate

182 models. Model differences in physics, but also in spin up procedures, the way

183 RCP scenarios are set up, and model climate sensitivities all likely contribute to

184 the model spread (Knutti and Hegerl, 2008; Szopa et al., 2013).

185   Vertical density profiles help to further explain the changes in stratification.

186 Mean vertical profiles of density in the 1990s and the density change between the

187 1990s and the 2090s show that all the models become more buoyant at the surface

188 as a consequence of heating and/or freshening of the upper ocean (Figure S1).

189 The density changes at the surface vary by almost a factor of two among models,

190 from -1.1 kg/m^3 (HadGEM-ES2) to -0.6 kg/m^3 (GFDL-ES2M), but converge to a

191 relatively narrow range (approximately -0.2 kg/m^3) at 500 m depth. Most of the

192 density change occurs between the surface and 200 m. Below 200 m, the density

193 change in most of the models varies linearly with depth. Thus, our definition of

194 the stratification index, as the density difference between the surface and 200 m,

195 is reasonable. The converging reductions in density among models at about 500

196 m agrees with some previous studies based on observations and CMIP3 models

197 (Bindoff et al., 2007; Lyman et al., 2010; Capotondi et al., 2012). Compared to

198 WOA09 data, the models generally underestimate the density of the upper ocean

199 in the top 150 m and most models overestimate the density below 350 m
200 (resulting in a positive stratification bias) (Figure S1a).

201   Vertical profiles of temperature and salinity from each model are also shown
202 in Figure S1. The surface ocean exhibits strong warming of 1.7-3.5°C by the 2090s
203 and the warming magnitude declines quickly with depth, which is associated
204 with the heat uptake capacity of individual models. For instance, the GFDL
205 models seem to be more efficient in transporting heat downward than the IPSL
206 models. Above 300 m, the temperature changes vary widely among the models.
207 Temperature changes as a function of depth are complex, and model-to-model
208 differences may be related to a number of factors including rates of vertical
209 mixing and the seasonal thermocline dynamics. At the depth of 500 m, the mean
210 temperature change converges at about 1.2°C. The ocean heat uptake capacity is
211 linked to ocean diapycnal mixing and other processes, such as mixing by
212 mesoscale eddies. The weak temperature gradients in the GFDL models suggest
213 high rate of heat uptake, and are consistent with ocean heat uptake estimates by
214 (Kuhlbrodt and Gregory, 2012). The large model spread in temperature profiles
215 suggests considerable differences and uncertainties in the parameterizations of
216 these physical processes across the models. Vertical profiles of salinity are more
217 scattered than for temperature (Figure S1c). In the 1990s, most of the models
218 underestimate salinity from the surface down to 550 m. Surface salinity is
219 generally biased low by 0.05-0.25 psu. Most of the freshening with climate
220 change takes place above 100 m, which also acts to increase stratification. Note
221 that the salinity increases at 100-300m in some models (IPSL, GFDL-ESM2M,
222 HadGEM2-ES) partially compensates the impact of rising temperatures on
223 density.

224   The percentage contribution of temperature change to the stratification

225   change from the 1990s to the 2090s is shown in Figure S2. Previous studies have

226   shown that salinity contributes significantly to the stratification changes at high

227   latitudes (>40°) in both hemispheres and in the North Pacific as a consequence of

228   increases in precipitation (Bindoff et al., 2007). From our comparisons,

229   temperature dominates the stratification changes in the tropical and sub-tropical

230   regions (Figure S2). Salinity dominates the stratification changes in the much of

231   the Arctic Ocean and in the high-latitude North Atlantic. While stratification is a

232   function of SSS and SST to a good approximation (Cabré et al., 2015),

233   stratification change at high latitudes is also dependent on temperature and

234   salinity at depth as vertical mixing and exchange are stronger.

235   In some regions the spatial distributions and the driving process differs

236   substantially across models. Generally, the models agree well in the tropics and

237   subtropical gyres that surface warming drives increasing stratification. In the

238   high latitude North Atlantic, the subpolar Pacific and the western Pacific Ocean,

239   there is weaker agreement across the models. In the subtropical gyre of the south

240   Pacific, stratification changes in the IPSL and CESM1(BGC) models have a

241   stronger influence from temperature change, while the other models exhibit

242   more complicated spatial patterns. In the North Atlantic, salinity contributes

243   more in the IPSL and HadGEM2 models than in the other models. The

244   southeastern Pacific is more dominated by salinity in the two GFDL models. In

245   the Southern Ocean, the models show relatively large contributions from both

246   salinity and temperature but with complicated spatial patterns that differ

247   considerably across models. Projections for the regions where the models do not

248   agree even on the driving factor should be viewed with more caution. Climate-

11

249   change and biogeochemical impacts in these regions tend to be projected with

250   less consistency across models (Bopp et al., 2013; Cabré et al., 2015).

251   Stratification increases globally in all the models with climate change

252   (Figures 1 and 2). Nearly all the models predict large increases in stratification in

253   the western tropical Pacific, the tropical Indian Ocean, the Arctic Ocean, and in

254   the high latitude North Atlantic (particularly in the Labrador Sea). The Southern

255   Ocean has weaker increases in stratification, partly because the surface layer

256   mixing and upwelling are intensified due to the poleward shift of strengthened

257   westerly jets (Swart and Fyfe, 2012). Our stratification index may underestimate

258   the changes in the high latitude North Atlantic, as the relatively deep mixing

259   means that temperature and salinity at 200m depth are changing much more

260   rapidly than in other regions. Reductions in the deep winter mixing and NADW

261   formation in this region are a common pattern seen in strong warming climate

262   simulations (e.g., Cheng et al., 2013; Schwinger et al., 2014). Less drastic increases

263   in stratification are seen over much of the rest of the oceans, with only a few

264   small regions showing decreases in some models. An exception is the HadGEM2-

265   ES model, which has large stratification reductions in the Arctic (Figure 2).

266   **3.2 Surface Nutrient Trends with Climate Change**

267   One of the key factors determining global NPP is nutrient availability in the

268   euphotic zone. Time series of global mean nutrient (0-100m) concentrations for

269   nitrate (NO_3), phosphate (PO_4), silicic acid (SiO_4) and dissolved iron (dFe) are

270   presented in Figure 3. The magnitude of surface nutrient concentrations differs

271   substantially across the models (varying by a factor of ~1.5-2, and by a factor of 5

272   for dissolved iron). The IPSL models have relatively low surface nutrient

273   concentrations. Compared to the WOA09, 2 models overestimate phosphate

274   (CESM1(BGC) and GFDL-ESM2G) and 5 models overestimate nitrate. All of the

275   models overestimate the silicic acid observations, with the exception of

276   CESM1(BGC). The CESM1(BGC) model overestimates surface phosphate

277   concentrations initially, due to excessive nitrogen limitation, but then shows the

278   strongest surface phosphate declines over the 21st century (Figure 4).

279   Over the entire period from 1850-2100, the models all display decreasing

280   trends for surface nitrate, phosphate and silicic acid. Interestingly, surface iron

281   concentrations increase modestly in all but one of the models, by 4-10%. Changes

282   in iron concentrations impact marine productivity, nitrogen fixation rates, and

283   oceanic net CO_2 uptake. In the CMIP5 simulations, iron inputs to the oceans from

284   deposition and rivers are held constant over time, so the increasing surface iron

285   concentrations may reflect increasing macronutrient limitation of phytoplankton

286   growth, leading to reduced biological uptake of iron. The reductions in the

287   sinking export flux also reduce the particle scavenging loss term for dissolved

288   iron. In the CESM1(BGC) model, increased production in the High Nutrient, Low

289   Chlorophyll (HNLC) regions offset about 25% of the reduction observed in the

290   macronutrient-limited areas with climate change, and changing circulation

291   patterns also altered the lateral transport of iron within the oceans (Moore et al.,

292   2013; Misumi et al., 2014).

293   The relative changes in nutrient concentrations (0-100m) (normalized to

294   1990s means) are presented in Figure 4. The relative changes in the historical run

295   show a consistent pattern across the models for nitrate, phosphate and dissolved

296   iron (except for HadGEM2-ES). In the RCP8.5 projection, the models show

297   diverging estimates of the magnitude of the relative changes. For nitrate, the

298   reductions range between 3% and 14%, whereas for phosphate the reductions

299   range between 3% and 20%. Silicic acid and iron trends are even more variable

300   than for nitrate and phosphate. For silicic acid, 3 models exhibit slight increases,

301   while the others exhibit decreases ranging from 5-17%. The variability in relative

302   change in silicic acid concentration in the RCP8.5 is likely associated with

303   changes in plankton community and variable diatom production (Bopp et al.,

304   2005). All of the models include some representation of diatoms (Table 2) but the

305   match to observed silicic acid concentrations for the current era is generally poor

306   (Figure 3).

307   The spatial distributions of mean nitrate concentration for 0-100 m in the

308   1990s are shown in Figure S3. The CMIP5 models reproduce key observed

309   features of the basin scale distributions of surface nitrate. For example, all of the

310   models exhibit elevated nitrate concentrations in the eastern equatorial Pacific,

311   Southern Ocean, subarctic North Atlantic and subarctic Pacific. In the subtropical

312   gyres of the Atlantic and Pacific basins, mean nitrate concentrations are low.

313   These general patterns are consistent with the WOA09 observations. However,

314   there are clear disagreements in some regions. For example, the details of the

315   high-nitrate surface water distributions vary considerably in the eastern

316   equatorial Pacific. The HNLC condition extends too far north and south of the

317   equator in some models, and too far to the west in others (Figure S3). The models

318   also differ in the intensity and extent of high nitrate concentration waters in the

319   subarctic North Pacific, where 6 of 9 models show lower nitrate concentrations

320   than the WOA09 data (MPI-ESM-LR, MPI-ESM-MR and HadGEM2-ES are

321   closest to the observations). There are also differences in the Arabian Sea and Bay

322   of Bengal, where most models underestimate nitrate concentrations except the

323   GFDL-ESM2M and MPI-ESM-LR models.

324   Inter-model spread in NPP during the 1990s is pronounced, with NPP as low

325   as 29 PgC yr^{-1} (IPSL-CM5A-LR and IPSL-CM5A-MR), while NPP in one model

326   exceeds 75 PgC yr^{-1} (GFDL-ESM2M) (Table 3, Figure 5). In addition, the spatial

14

327 pattern of NPP is not well represented by the multi-model mean (Bopp et al.,

328 2013). Satellite based estimation of NPP is approximately 50 PgC yr^{-1} (Behrenfeld

329 et al., 2006; Carr et al., 2006). The MPI-ES-MR and CESM1(BGC) models had NPP

330 of 49.8 PgC yr^{-1} and 54.2 PgC yr^{-1}, closer to the satellite-based estimates, and the

331 observationally constrained, model estimate of 56 PgC yr^{-1} by Buitenhuis et al.

332 (2013). The magnitude of EP also varies substantially across models in the 1990s,

333 ranging from 4.4 to 7.2 PgC yr^{-1} (Table 3).

334 **3.3 Climate Change Impacts on NPP and EP**

335 All of the models exhibit decreasing trends in global NPP and EP with

336 climate change, as shown in previous studies (Bopp et al., 2013; Dutkiewicz et al.,

337 2013) and most models show more rapid decreases during the middle to latter

338 part of the 21st century (Figures 5-6, Table 3). All nine models project decreases in

339 export production by the 2090s, exceeding 5% relative to levels in the 1990s,

340 whereas the response for NPP is divided into 2 groups after 2020. The

341 CESM1(BGC) and GDFL models experience smaller changes in NPP (< 5%

342 relative to 1990s) while other models have larger decreases (8-16%). The largest

343 relative change for NPP is about -16% (MPI-ESM-LR). The EP decreases range

344 from 7% for GFDL-ESM2G to 28% for IPSL-CM5A-LR. Cabré et al. (2015) found

345 reductions in NPP and EP for all biomes, except at the highest latitudes. The

346 reductions in global NPP and EP co-vary with the increases in stratification

347 (Figure 6). By the 2090s, stratification increases by about 16% in GFDL-ESM2M

348 and up to 33% in HadGEM1-ES. The rate of stratification increase is slower in the

349 two GFDL models and CESM1(BGC), which also agrees with the slower rates of

350 relative NPP and EP change.

351 The variability across models in NPP is substantially larger than that seen in

352 EP (Table 3). The normalized standard deviation was ± 27 % for NPP, but only ±

353   12 % for EP in the 1990s. The large spread in simulated NPP and its response to
354   climate change was also noted by (Laufkötter et al., 2015). Seven of the nine
355   models have an EP between 6.0 and 7.2 PgC yr^{-1} in the 1990s, with the remaining
356   two (HadGEM2-ES and GFDL-ESM2G) having considerably lower EP (< 5 PgC
357   yr^{-1}). EP is tightly coupled to new nutrient inputs to the euphotic zone in these
358   models. NPP is less tightly coupled as the fraction of regenerated production
359   varies across the models, and can vary spatially and temporally within some
360   models. Thus, the large spread in NPP is not just a function of the different
361   physical models and their transport of nutrients to the euphotic zone, but rather
362   it is also strongly impacted by the phytoplankton community structure and
363   export efficiency inherent in the models, and the resulting varying levels of
364   regenerated production.

365   The sinking carbon flux out of the euphotic zone to net primary production
366   ratio (particle export ratio or pe-ratio) is a measure of the export efficiency and
367   also reflects the variable contribution of regenerated production to total NPP
368   (Dugdale and Goering, 1967; Eppley and Peterson, 1979; Dunne et al., 2007).
369   High pe-ratio values are typically associated with productive ecosystems
370   dominated by larger phytoplankton (often diatoms; Buesseler, 1998; Boyd and
371   Newton, 1999), while low pe-ratios are associated with oligotrophic food webs
372   with most carbon flow through the microbial loop (Pomeroy, 1974; Azam et al.,
373   1983). The CMIP5 models that include both large and small phytoplankton,
374   assume a higher export efficiency for the large phytoplankton (Aumont and
375   Bopp, 2006; Seferian et al., 2013; Tjiputra et al., 2013). The fraction of grazed
376   material routed to sinking export is higher, often by a factor of 3 or more, than
377   the fraction routed to sinking export for the small phytoplankton. Diatoms are
378   also likely to dominate phytoplankton blooms in these models. This can drive

379 additional, very efficient, export through aggregation, further enhancing the

380 differences in export efficiency between large and small phytoplankton. Relative

381 to the 1990s, six of the nine models show decreasing trends in the pe-ratio (up to

382 a 10% reduction) (Figures 5-6, Table 3; see also Cabré et al., 2015). Diatoms

383 account for a smaller percentage of NPP in the 2090s than in the 1990s in all the

384 models, except for the MPI model, where nearly all of the production is by

385 diatoms and the smallest phytoplankton are not explicitly represented (Table 3).

386 **3.4 Increasing Stratification and Declining Nutrients, NPP, and EP**

387 We quantify the relations between stratification and key biogeochemical

388 variables with annual model output over the entire time period of 1850-2100.

389 This approach captures physical-biological interactions over interannual to

390 centennial timescales, and is thus more robust than the earlier work comparing

391 two end points from the beginning and end of the 21st century (Bopp et al., 2013;

392 Cabré et al., 2015). Changes in global NPP relative to the 1990s are plotted

393 against the relative change in stratification in Figure 7a. Across all the ESMs, a

394 relatively good relationship exists with a correlation r^2=0.72. Larger relative

395 increases in stratification correspond to larger relative declines in NPP. In

396 addition, the globally-fitted line with a slope of 0.38 separates the models into

397 two groups. In one group (GFDL, IPSL and CESM1(BGC)), the NPP reductions

398 are more modest as stratification increases; the other group is composed of the

399 two MPI models, HadGEM1-ES and the NorESM model, which show more

400 intense and linear reductions in NPP with increasing stratification. The reduction

401 of NPP can be partly explained by nutrient changes responding to stratification

402 increases. Across the models, surface nitrate and phosphate concentrations

403 clearly decline as the stratification is enhanced (Figure 7c and 7d, with r^2 of 0.80

404 and 0.82, respectively). Note that all of these trends are robust across the full time

405   series. Compared to the 1990s, the preindustrial stratification is weaker, surface

406   nutrient concentrations are higher, and NPP and EP are elevated (Figures 3-7).

407   This indicates significant climate change impacts on ocean biogeochemistry,

408   prior to the 1990s and the modern era when most ocean observations have been

409   made. The response of surface silicic acid to increasing stratification is more

410   variable. The projected changes are more divided, as three models (MPI-ESM-LR,

411   MPI-ESM-MR and HadGEM1-ES) show slight increases and the others show

412   reductions in surface silicic acid concentrations (Figure 7b).

413   EP is even more closely related to the stratification changes (r^2=0.89) than

414   NPP (r^2=0.72; Figure 7e). The EP change is also closely related to the NPP change

415   (r^2=0.85) . EP decreases by up to 20% (Figure 7e) whereas NPP decreases by 10-

416   18%. The models display two patterns in terms of the response of NPP and EP to

417   climate change. The first group includes five models (the two IPSL models,

418   CESM1(BGC) and the two GFDL models) where the relative declines in NPP are

419   smaller than the relative declines in EP by a factor of 2 or more (Figure 6 and

420   Table 3). In this group, the EP drops by about 10% and the NPP decreases by 5% .

421   In the remaining models the relative declines in EP and NPP are larger and more

422   similar in magnitude. For example, both EP and NPP decrease by about 14% in

423   the HadGEM2-ES model. The differential declines in NPP and EP in the first

424   group of models documents declining export efficiency for the ocean biological

425   pump, driven by phytoplankton community shifts and a decreased contribution

426   to NPP by large phytoplankton (diatoms) (see below and Figures 6-10; also Cabré

427   et al., 2015).

428   Reduced nutrient availability is a major contributor to the declines in NPP

429   and EP. However, the relationship varies from one model to another because

430   growth and export are complicated functions of macronutrient limitation,

18

431 temperature, irradiance and iron limitation, as well as the routing of organic

432 matter within the ecosystem that drives export efficiency. Higher metabolic rates

433 with warming can be compensated to a large degree by changes in the supply of

434 nutrients in terms of globally integrated productivity (Dutkiewicz et al., 2013).

435 The NPP response is also strongly impacted by phytoplankton community

436 structure, which modifies export efficiency, and the corresponding magnitude of

437 regenerated primary production. For the IPSL, CESM1(BGC), and GFDL models

438 that show larger declines in EP than in NPP, this pattern is driven by a

439 decreasing contribution to total NPP by large phytoplankton (Table 3, Figures 8-

440 9). Most of the primary production in these models is by smaller phytoplankton.

441 The GFDL models express this pattern most strongly, with minimal declines in

442 NPP, despite declines in EP approaching 10% (Figure 6 and Table 3). The other

443 models tend to have production that is dominated by diatoms, and do not

444 capture the community shifts towards increasing small phytoplankton

445 dominance (and reduced export efficiency) under increasing nutrient stress. The

446 declines in NPP with increasing stratification are more linear and more similar in

447 magnitude to the declines in EP (Figure 7, panels a, b, and h). Thus, there are also

448 very strong correlations between the climate-driven changes in the fractional

449 contribution of diatoms to NPP and both the changes in stratification and the

450 changes in EP (Figure 7, panels f and g, correlations of r^2=0.85 and r^2=0.95, both

451 much higher than the correlation between changing stratification and NPP,

452 r^2=0.71). Cabré et al. (2015) found similar patterns relating community

453 composition, NPP, and EP comparing the period from 1980-1999 with 2080-2099,

454 across low to mid-latitude biomes.

455 Some of these patterns are illustrated in Figure 8, which shows the

456 contribution of diatoms (large phytoplankton) to NPP for the 1990s. Most of the

457 models show elevated diatom production at high latitudes and low diatom

458 contributions in the subtropical gyres. However, there are large discrepancies in

459 the magnitude of the diatom contribution, ranging from about 30% to more than

460 90% in the Arctic Ocean, for example. At the global-scale diatoms account for

461 only 9.4% of NPP in the GFDL-ESM2M model and reach a maximum of 91% in

462 the MPI-ESM-MR model (Table 3). The large variability across the models

463 reflects, in part, the lack of observational datasets to constrain phytoplankton

464 community composition, at the time these models were being developed. The

465 new globally-gridded ocean atlas of plankton functional types, Marine

466 Ecosystem Data (MAREDAT) (Buitenhuis et al., 2013) has started to fill this gap,

467 and should lead to improved representations of plankton community structure

468 in the future as the dataset becomes increasingly populated and is entrained into

469 model development and validation. Remote sensing estimates of phytoplankton

470 community composition and size class structures are also providing useful

471 constraints for global-scale modeling efforts (e.g., Alvain et al., 2005; Hirata et al.,

472 2008; Kostadinov et al., 2009; Siegel et al., 2014).

473   The spatial patterns of the shifts in phytoplankton community composition

474 with climate change are illustrated in Figure 9; which shows the change in the

475 percentage of NPP by diatoms (2090s – 1990s). There are some robust trends

476 across the models. One of the areas with the biggest declines in diatom

477 production is the high-latitude North Atlantic. This region typically has some of

478 the biggest stratification increases with climate change, greatly reducing the deep

479 winter mixing that entrains nutrients to the surface (Moore et al., 2013;

480 Randerson et al., 2015). Nearly all the models also show large declines in diatom

481 contributions to production in the Arctic Ocean. The CMIP5 models show

482 consistent trends of increasing stratification, declining surface nutrient

483 concentrations, and a longer growing season with climate change in the Arctic

484 (Vancoppenolle et al., 2013). Increasing surface temperatures and substantial

485 declines in sea ice cover allow for a longer growing season with climate change.

486 Thus, nutrients in surface waters are more completely used up by summer's end,

487 leading to community shifts with decreased diatom production and an increased

488 fraction of production by smaller phytoplankton. In the CESM1(BGC) model, this

489 community shift allows for a small increase in central Arctic NPP, even as export

490 production and surface nutrient concentrations decline, due to the increased

491 fraction of NPP from small phytoplankton and the resulting increases in

492 regenerated production (Moore et al., 2013).

493   All of the models show some increase in the fraction of NPP by diatoms in

494 the Southern Ocean (Figure 9). The increase is particularly strong in the

495 CESM1(BGC), IPSL, and GFDL models. Most of the models also show some

496 increased diatom production in the tropical Pacific. Bopp et al. (2005) reported

497 decreasing diatom production in the Arctic and high-latitude North Atlantic,

498 with some increases in the Southern Ocean under a strong warming climate

499 scenario. (Steinacher et al., 2010) also found declining productivity in the North

500 Atlantic, and shifts in the export ratio due to phytoplankton community shifts

501 with decreasing diatom production. An earlier version of the CESM used in that

502 study (CCSM3) showed only small shifts in export ratios with climate change, as

503 the range in export ratios and the differences in export efficiencies between large

504 and small phytoplankton were smaller than in CESM1(BGC) (Steinacher et al.,

505 2010; Moore et al., 2013). Three models in this study (HadGEM2-ES and the two

506 MPI models) show increases in diatom production in the low latitudes (Figure 9).

507 However, the diatoms dominate production nearly everywhere in these three

508 models (Figure 8).

509   There are also large inter-model differences in the spatial patterns of the pe-

510   ratio (Figure 10). Some of the models (GFDL, IPSL, CESM1(BGC)) show a close

511   correlation between the pe-ratio and diatom production (compare Figures 8 and

512   10), due to the enhanced export efficiency for diatoms (large phytoplankton)

513   built into the models. Thus, there is a very high correlation between the changing

514   contribution of diatoms to NPP and the changes in EP (Figure 7, panel g, Table 3).

515   The MPI model includes one phytoplankton group and has an essentially

516   constant pe-ratio of 0.15, explaining the linearity of the changes in NPP and EP

517   with warming (Figures 8 and 10). Production in the HadGEM1-ES model is

518   dominated nearly everywhere by the diatoms (Figure 8). Therefore, the MPI and

519   HadGEM models cannot capture a shift towards increasing small phytoplankton

520   dominance under declining surface nutrient concentrations. This leads to export

521   production being closely correlated with diatom production in these models as

522   most production is by diatoms, as well as in the other models where diatoms are

523   assumed to export more efficiently but account for a smaller fraction of total NPP

524   (Table 3).

525   There is also a strong correlation between the declines in the fraction of NPP

526   by diatoms and declines in the pe-ratio (compare Figures 7, 9 and 11). The largest

527   declines in the pe-ratio are seen in the Arctic and the high-latitude North Atlantic,

528   regions where diatom production also decreases the most. The GFDL, IPSL, and

529   CESM1(BGC) models show some reductions in pe-ratio in the subarctic North

530   Pacific, but the spatial patterns are inconsistent (Figure 11). The models display

531   considerable variability in the degree of stratification increase and in the

532   dominant factor driving these changes in the subarctic North Pacific (Figures S2

533   and 2).

534   The correlation for the relationship between the changing percentage of NPP

535   by diatoms versus the changes in EP across all the models has an r^2 of 0.96 and a

536   slope close to 1 (0.94, Figure 7g), indicating that phytoplankton community

537   structure plays a dominant role in determining the responses of NPP, EP, and the

538   pe-ratio to climate change. The biggest declines in the fraction of production by

539   diatoms and pe-ratios are in precisely the areas where some of the largest

540   increases in upper ocean stratification are seen, along with declining surface

541   nutrient concentrations, as in the Arctic Ocean and in the high latitude North

542   Atlantic (Figures 6-8; see also Steinacher et al. (2010); Moore et al. (2013)).

543   **3.5 Projected Changes in NPP, EP and Stratification Biases**

544   At the global scale, the CMIP5 models show considerable stratification biases

545   for the 1990s when compared to the WOA09 data (Figure 1, Table 3). Only the

546   GFDL-ESM2M model is within 10% of the observed value. From the density

547   profiles as well (Figure S1) it is apparent that most of the models have stronger

548   stratification in the 1990s than seen in the observations. Liu et al. (2014) argue

549   that climate bias is important when projecting the impact of climate change on

550   land surface processes and Hoffman et al. (2014) document this for atmospheric

551   CO_2 mole fractions. Here, we examine how stratification biases in the 1990s may

552   affect model projections of NPP and EP in the 2090s.

553   Models with stronger bias in the 1990s for surface stratification tend to

554   predict larger climate-induced declines in both NPP and EP (Figure 12, r^2=0.47

555   and r^2=0.54, respectively). The slopes are plotted when the correlation is

556   significant at >95% level. Five of the models have positive biases in stratification

557   for the current era that exceed 20%. These models also show the largest relative

558   increases in stratification with climate change of 26-30% (Figure 12, Table 3). The

559   remaining four models (GFDL models, CESM1(BGC), and NorESM1-ME) do a

560   better job of simulating observed stratification for the current era, and predict
561   relative increases in stratification over the 21st century that are roughly half as
562   large, ranging from ~15-18%. This suggests that the more biased models (for the
563   1990s) may be overestimating the projected reductions in NPP and EP for the end
564   of the century.

565

566   **4 Discussion and Conclusions**

567   The ESMs analyzed here have different resolutions and incorporate marine
568   biogeochemical-ecosystem models with different mechanisms and degrees of
569   complexity. We find this set of models has consistent trends of increasing
570   stratification and decreasing NPP and EP. However, a large model spread is
571   apparent for the 1990s, particularly for NPP, and in the relative changes to NPP
572   and EP over the 21st century due to climate change. NPP is reduced by 2-18% in
573   the 2090s and EP is reduced by 7-20%. Mean stratification increased by 16%
574   (GFDL-ESM2M) up to 33% (HadGEM1-ES) from the 1990s to the 2090s. Under
575   strong warming scenarios like RCP8.5, ocean stratification will continue to
576   rapidly increase after the year 2100 in all of these models (Randerson et al., 2015).

577   The strongly linear relationship between stratification increases and EP
578   decreases seen within each model and across all the models (Figures 7 and 12)
579   indicates a strong bottom up control on EP, through declining upward nutrient
580   flux to the euphotic zone. Declining surface nutrient concentrations are seen in
581   all the models with climate change under the RCP 8.5 scenario (Figures 5-6).
582   Nitrate is reduced by 3 to 14% and phosphate is reduced by 3 to 20%. Changes in
583   surface silicic acid and iron concentrations are more variable across the models.
584   For silicic acid, there are 3 models showing slight increases, while the others
585   exhibit decreases of 5-17%. With respect to iron, 8 models indicate an increase of

24

586   4-10% relative to the 1990s; with the exception being the NorESM-ME model,
587   which is reduced by 3%. Changes in the temperature and light fields also have
588   impacts on EP in some regions, but increasing stratification and nutrient stress,
589   and the resulting impacts on phytoplankton community composition and EP is
590   the dominate process at the global scale. On a global scale, over the full 1850-2100
591   time period, the changes in NPP and EP are more highly correlated with the
592   changes in stratification, than with the changes in SST (r^2 0.72 for stratification-
593   NPP and 0.66 for SST-NPP, Figure 7). This is because that the stratification metric
594   captures both the temperature-driven changes that dominate at low to mid-
595   latitudes, and the salinity-driven changes at higher latitudes. The temperature-
596   driven increases in growth rates are partially offset by reduced nutrient supply
597   in many regions as stratification increases (Bopp et al., 2005; Cabré et al., 2015).

598   Simulated NPP and its response to climate change are both more variable
599   across the models than EP, and are less strongly correlated with changes in
600   stratification (Figure 7). This is driven by model differences in the export
601   efficiency of the biological pump and its relation to phytoplankton community
602   structure. The models that allow for shifts in phytoplankton community
603   structure show strongly non-linear NPP response to climate change. NPP
604   declines less rapidly than EP with increasing nutrient stress, as the percentage of
605   NPP by large cells declines and export efficiency decreases (and the regenerated
606   production fraction increases). Models without this dynamic community
607   composition and export efficiency show a much more linear NPP response to
608   climate change (Figure 7). Thus, projections of the response of NPP to climate
609   change in the CMIP5 models are critically dependent on the simulated
610   phytoplankton community structure, the efficiency of the biological pump, and
611   the resulting (highly variable) levels of regenerated production.

612   Spatial patterns of diatom productivity are influenced by changes in surface

613   nutrients and the resulting shifts in plankton community composition. The

614   response of the %NPP by diatoms depends on several factors, including whether

615   they were a small or large component of the community initially. Therefore, the

616   spatial patterns of changes in stratification and %NPP by diatoms can differ

617   (Figure 2 and Figure 9). The largest decreases are seen in areas with high diatom

618   production initially and large increases in stratification, particularly in the

619   Northern Hemisphere, leading to a North-South hemispheric asymmetry

620   (Marinov et al., 2013; Cabré et al., 2015). In the Southern Ocean, the winds that

621   drive upwelling, strengthen and shift poleward with climate change, influencing

622   iron supply and productivity patterns (Moore et al., 2013; Misumi et al., 2014).

623   The large spread in the simulated NPP rates for the 1990s and the variability

624   seen across models in the response of NPP to climate change introduce

625   challenges for climate impact and risk assessment, as NPP is a key product of

626   both terrestrial and marine ecosystem models, and changes to NPP are perhaps

627   the most cited result from this class of models. We have demonstrated that the

628   wide spread seen in simulated NPP is not due to the different physical

629   circulation models and the flux of nutrients they deliver to surface waters, but

630   rather to the efficiency of the biological pump (tied to community structure in

631   most models) and the resulting levels of regenerated primary production.

632   Changes in EP are an additional useful metric of climate impacts on marine

633   ecosystems. EP is more strongly tied to the climate feedback, as it is mainly the

634   fixed carbon sequestered to the deeper ocean by the biological pump that will

635   impact air-sea CO_2 exchange. In addition, in terms of impacts up the food chain,

636   EP may be a better metric than NPP. Friedland et al. (2012) demonstrated that

637   there is no correlation between fishery yield and NPP at the global scale, but that

there are strong correlations between fishery yield and several other variables including chlorophyll concentration, the pe-ratio, and EP. These three proxies all correlate with the fraction of primary production by large phytoplankton. In this context, the results presented here suggest large future declines in fishery yield across the high-latitude North Atlantic.

Laufkötter et al. (2015) suggest a strong impact of temperature modification of phytoplankton growth rates and other ecosystem processes (including zooplankton growth and grazing rates) to infer a strong top-down grazing influence on the NPP response to climate change, noting that phytoplankton growth rates appear to increase at low latitudes in some models, even as available nutrient concentrations decline. However, many of the key fluxes and fields needed to support this hypothesis were not available in the archived output from the CMIP5 models. This study relied on estimated nutrient limitation factors and growth rates for only the surface ocean in their analysis. Temperature warming is strongest at the surface (Figure 1S). Thus, the analysis may overestimate the temperature impacts for the whole euphotic zone. Their conclusions were based on diatom-specific nutrient limitation patterns, on the phytoplankton group with the largest changes in limitation factors, and on comparing total grazing with total NPP for some models (Figures 6-8, Laufkötter et al. (2015)). These may not be representative of the community nutrient limitation patterns and growth response. At low latitudes the diatoms might show the biggest declines in growth due to nutrient limitation, but they are only a small component of the community in many of the models (Figure 8). Under increasing nutrient stress, phytoplankton community growth rates may increase simply due to a declining contribution from diatoms, as the smaller phytoplankton will typically grow faster at low nutrient concentrations. Grazing

664   rates are also higher on the small phytoplankton in models with multiple groups.

665   Thus, comparing total grazing rates to NPP cannot account for these influences

666   of phytoplankton community shifts. A community shift towards smaller

667   phytoplankton will likely increase mean community growth rate and total

668   grazing, even with no change in temperature.

669   We agree that temperature effects may be important in the NPP climate-

670   change response, and that the temperature influence on phytoplankton growth

671   rates, and on the ecosystem processing of NPP that leads to export, are highly

672   uncertain (Laufkötter et al., 2015). Sherman et al. (2016) compiled in situ

673   estimates of phytoplankton community growth rates at the global-scale, and

674   found a relatively weak apparent temperature effect (apparent Q_{10} ~ 1.5). These

675   observational estimates of phytoplankton community growth rates were

676   compared with the CESM and GFDL CMIP5 simulations analyzed here. ESMs

677   used in climate change studies need to ensure that the emergent, community

678   temperature-growth relation matches this observed value (even though higher

679   explicit Q10 values may be prescribed for individual plankton functional types)

680   to avoid biases in the response to temperature change (Sherman et al., 2016).

681   Some of the CMIP5 models have an assumed higher export efficiency for

682   diatoms relative to small phytoplankton, building on a long-standing paradigm,

683   strengthened by results from the detailed ecosystem studies of the Joint Global

684   Flux Study (JGOFS) program (Buesseler, 1998; Boyd and Newton, 1999). In the

685   current models, the spectrum of phytoplankton size structure is often

686   represented very simply with only the end members of one large and one small

687   phytoplankton group. Thus, the "diatom" group is a proxy for larger, efficiently-

688   exporting, blooming phytoplankton functional types. DOM cycling,

28

689   heterotrophic bacteria, microzooplankton, and the microbial loop are typically

690   treated in an idealized, implicit manner in the current models as well.

691   To accurately predict the response of NPP and EP to climate change, it may

692   be necessary to develop more robust ecosystem models with additional explicit

693   phytoplankton, heterotrophic microbial, and zooplankton groups, including their

694   impacts on nutrient cycling, export efficiency and the downward transport of

695   organic matter. Models that include much greater diversity in the phytoplankton,

696   show large community composition shifts with climate change (Dutkiewicz et al.,

697   2013). Quantifying the links between NPP, EP and community composition in

698   observational datasets is a high priority. There are only limited field observations

699   of the pe-ratio, some of which rely on nutrient drawdown and other indirect

700   estimates of the sinking particle flux (Dunne et al., 2007). Further progress to

701   improve model performance requires combined efforts from satellite, field, and

702   laboratory observations, empirical and inverse modeling approaches, as well as

703   process-based, forward models.

704   The large model spread in EP and NPP, and significant biases seen in key

705   nutrient fields for the 1990s suggest that the current ocean biogeochemical

706   models are far from perfect and their results must be interpreted with caution.

707   However, the relationships between stratification and EP, NPP and nutrients do

708   reveal some common mechanisms driving the climate change response. The

709   large inter-model differences for the current era in NPP, EP and nutrient

710   concentrations are partially associated with how these biogeochemical models

711   are initialized and spun up for these experiments. The ocean biogeochemical

712   models are often integrated in an offline mode for a thousand years or more

713   before coupling to other components of the ESM (Séférian et al., 2016). The

714   achieved preindustrial, near-steady state of biogeochemical fields may deviate

715 substantially from the observed climatology, driven by biases in the physics and

716 biogeochemistry. These differences typically persist in the present-day

717 simulations and future projections. The advantage of the initialization and spin

718 up process is that the biogeochemical fields are consistent with the simulated

719 ocean circulation, and will respond to climate-driven changes appropriately. The

720 strong intrinsic variability helps to reduce model drift and generate reasonable

721 longer-term variability. As a result, these long-term simulations are suitable for

722 analyzing climate trends, variability and sensitivities. RCP 8.5 is a strong

723 warming scenario and the relationship between stratification changes and

724 NPP/EP changes may be somewhat different under other RCP scenarios.

725 Although the relations between the degree of surface warming and the ocean

726 biogeochemical responses were largely linear across RCP 4.5 and 8.5 for the

727 CESM(BGC) (Moore et al., 2013).

728 Some potentially important marine biogeochemical feedbacks on the climate

729 system were missing completely or not well represented in the CMIP5 models,

730 including important feedbacks through aerosol transport and deposition on the

731 marine iron cycle, feedbacks involving the oxygen minimum zones and the

732 marine nitrogen cycle, and the impacts on ocean biology by ongoing ocean

733 acidification. Each of these feedbacks could impact phytoplankton and

734 zooplankton community structures, NPP, EP, and pe-ratios in the future.

735 It is also important to consider the longer-term climate change responses of

736 both ocean physics and marine biogeochemistry. Moore et al. (2013) noted that

737 climate impacts on the oceans were still accelerating at year 2100 under the RCP

738 8.5 scenario (but not under the more moderate RCP 4.5 scenario). Randerson et al.

739 (2015) extended the CESM1(BGC) RCP 8.5 scenario simulation examined here, to

740 the year 2300. In these longer simulations, the climate impacts on ocean physical

741 fields and biogeochemistry lead to even stronger perturbations after 2100 than

742 those presented here. In addition, the ocean contribution to the climate-carbon

743 feedback exceeded the land contribution after the year 2100 (Randerson et al.,

744 2015).

745

746 **<u>5 Acknowledgments</u>**

756

757

758   **6 References**

759   **Uncategorized References**

760   Alvain, S., Moulin, C., Dandonneau, Y., and Breon, F. M.: Remote sensing of

761   phytoplankton groups in case 1 waters from global SeaWiFS imagery, Deep-Sea

762   Research Part I-Oceanographic Research Papers, 52, 1989-2004, 2005.

763   Aumont, O. and Bopp, L.: Globalizing results from ocean in situ iron fertilization

764   studies, Global Biogeochemical Cycles, 20, GB2017,doi:2010.1029/2005GB002591,

765   2006.

766   Azam, F., Fenchel, T., Field, J. G., Gray, J. S., Meyerreil, L. A., and Thingstad, F.:

767   The Ecological Role Of Water-Column Microbes In The Sea, Marine Ecology

768   Progress Series, 10, 257-263, 1983.

769   Behrenfeld, M. J., O'Malley, R. T., Siegel, D. A., McClain, C. R., Sarmiento, J. L.,

770   Feldman, G. C., Milligan, A. J., Falkowski, P. G., Letelier, R. M., and Boss, E. S.:

771   Climate-driven trends in contemporary ocean productivity, Nature, 444, 752-755,

772   2006.

773   Bindoff, N. L., Willebrand, J., Artale, V., Cazenave, A., Gregory, J. M., Gulev, S.,

774   Hanawa, K., Le Quéré, C., Levitus, S., and Nojiri, Y.: Observations: oceanic

775   climate change and sea level. Cambridge University Press, Cambridge, 2007.

776   Bopp, L., Aumont, O., Cadule, P., Alvain, S., and Gehlen, M.: Response of

777   diatoms distribution to global warming and potential implications: A global

778   model study, Geophysical Research Letters, 32, L19606,

779   doi:19610.11029/12005gl023653, 2005.

780   Bopp, L., Monfray, P., Aumont, O., Dufresne, J. L., Le Treut, H., Madec, G.,

781   Terray, L., and Orr, J. C.: Potential impact of climate change on marine export

782   production, Global Biogeochemical Cycles, 15, 81-99, doi: 10.1029/1999gb001256,

783   2001.

784　Bopp, L., Resplandy, L., Orr, J. C., Doney, S. C., Dunne, J. P., Gehlen, M.,

785　Halloran, P., Heinze, C., Ilyina, T., Seferian, R., Tjiputra, J., and Vichi, M.:

786　Multiple stressors of ocean ecosystems in the 21st century: projections with

787　CMIP5 models, Biogeosciences, 10, 6225-6245, doi: 6210.5194/Bg-6210-6225-2013,

788　2013.

789　Boyd, P. W. and Newton, P. P.: Does planktonic community structure determine

790　downward particulate organic carbon flux in different oceanic provinces?, Deep-

791　Sea Research Part I-Oceanographic Research Papers, 46, 63-91, 1999.

792　Buesseler, K. O.: The decoupling of production and particulate export in the

793　surface ocean, Global Biogeochemical Cycles, 12, 297-310, doi:

794　210.1029/1097gb03366, 1998.

795　Buitenhuis, E., Vogt, M., Moriarty, R., Bednarsek, N., Doney, S., Leblanc, K., Le

796　Quéré, C., Luo, Y.-W., O'Brien, C., and O'Brien, T.: MAREDAT: towards a world

797　atlas of MARine Ecosystem DATa, Earth System Science Data, 5, 227-239, 2013.

798　Cabré, A., Marinov, I., and Leung, S.: Consistent global responses of marine

799　ecosystems to future climate change across the IPCC AR5 earth system models,

800　Climate Dynamics, 45, 1253-1280, doi: 1210.1007/s00382-00014-02374-00383, 2015.

801　Capotondi, A., Alexander, M. A., Bond, N. A., Curchitser, E. N., and Scott, J. D.:

802　Enhanced upper ocean stratification with climate change in the CMIP3 models,

803　Journal of Geophysical Research-Oceans, 117, C04031,

804　doi:04010.01029/02011JC007409, 2012.

805　Carr, M.-E., Friedrichs, M. A. M., Schmeltz, M., Aita, M. N., Antoine, D., Arrigo,

806　K. R., Asanuma, I., Aumont, O., Barber, R., Behrenfeld, M., Bidigare, R.,

807　Buitenhuis, E. T., Campbell, J., Ciotti, A., Dierssen, H., Dowell, M., Dunne, J.,

808　Esaias, W., Gentili, B., Gregg, W., Groom, S., Hoepffner, N., Ishizaka, J., Kameda,

809　T., Le Quere, C., Lohrenz, S., Marra, J., Melin, F., Moore, K., Morel, A., Reddy, T.

810　E., Ryan, J., Scardi, M., Smyth, T., Turpie, K., Tilstone, G., Waters, K., and

811   Yamanaka, Y.: A comparison of global estimates of marine primary production

812   from ocean color, Deep-Sea Research Part Ii-Topical Studies in Oceanography,

813   53, 741-770, 2006.

814   Cheng, W., Chiang, J. C. H., and Zhang, D.: Atlantic Meridional Overturning

815   Circulation (AMOC) in CMIP5 Models: RCP and Historical Simulations, J

816   Climate, 26, 7187-7197, 2013.

817   Dugdale, R. C. and Goering, J. J.: Uptake of new and regenerated forms of

818   nitrogen in primary productivity, Limnology and Oceanography, 12, 196-206,

819   1967.

820   Dunne, J. P., Sarmiento, J. L., and Gnanadesikan, A.: A synthesis of global

821   particle export from the surface ocean and cycling through the ocean interior and

822   on the seafloor, Global Biogeochemical Cycles, 21, GB4006,

823   doi:4010.1029/2006GB002907, 2007.

824   Dutkiewicz, S., Scott, J. R., and Follows, M. J.: Winners and losers: Ecological and

825   biogeochemical changes in a warming ocean, Global Biogeochemical Cycles, 27,

826   463-477, doi 410.1002/Gbc.20042, 2013.

827   Eppley, R. W. and Peterson, B. J.: Particulate Organic-Matter Flux And

828   Planktonic New Production In The Deep Ocean, Nature, 282, 677-680, 1979.

829   Friedland, K. D., Stock, C., Drinkwater, K. F., Link, J. S., Leaf, R. T., Shank, B. V.,

830   Rose, J. M., Pilskaln, C. H., and Fogarty, M. J.: Pathways between primary

831   production and fisheries yields of large marine ecosystems, PLoS One, 7, e28945,

832   2012.

833   Fung, I. Y., Doney, S. C., Lindsay, K., and John, J.: Evolution of carbon sinks in a

834   changing climate, Proceedings of the National Academy of Sciences of the United

835   States of America, 102, 11201-11206, 2005.

836   Goldstein, B., Joos, F., and Stocker, T. F.: A modeling study of oceanic nitrous

837   oxide during the Younger Dryas cold period, Geophysical Research Letters, 30,

838   1092, 1010.1029/2002gl016418, 2003.

839   Hannon, E., Boyd, P. W., Silvoso, M., and Lancelot, C.: Modeling the bloom

840   evolution and carbon flows during SOIREE: Implications for future in situ iron-

841   enrichments in the Southern Ocean, Deep-Sea Research Part Ii-Topical Studies in

842   Oceanography, 48, 2745-2773, 2001.

843   Hauck, J. and Volker, C.: Rising atmospheric CO_2 leads to large impact of

844   biology on Southern Ocean CO_2 uptake via changes of the Revelle factor,

845   Geophysical Research Letters, 42, 1459-1464, doi: 1410.1002/2015gl063070, 2015.

846   Hirata, T., Aiken, J., Hardman-Mountford, N., Smyth, T. J., and Barlow, R. G.: An

847   absorption model to determine phytoplankton size classes from satellite ocean

848   colour, Remote Sens Environ, 112, 3153-3159, 2008.

849   Hoffman, F. M., Randerson, J. T., Arora, V. K., Bao, Q., Cadule, P., Ji, D., Jones, C.

850   D., Kawamiya, M., Khatiwala, S., Lindsay, K., Obata, A., Shevliakova, E., Six, K.

851   D., Tjiputra, J. F., Volodin, E. M., and Wu, T.: Causes and implications of

852   persistent atmospheric carbon dioxide biases in Earth System Models, Journal of

853   Geophysical Research-Biogeosciences, 119, 141-162, doi: 110.1002/2013JG002381,

854   2014.

855   Ito, T., Bracco, A., Deutsch, C., Frenzel, H., Long, M., and Takano, Y.: Sustained

856   growth of the Southern Ocean carbon storage in a warming climate, Geophysical

857   Research Letters, 42, 4516-4522, doi: 4510.1002/2015gl064320, 2015.

858   Jin, X., Gruber, N., Dunne, J. P., Sarmiento, J. L., and Armstrong, R. A.:

859   Diagnosing the contribution of phytoplankton functional groups to the

860   production and export of particulate organic carbon, $CaCO_3$, and opal from

861   global nutrient and alkalinity distributions, Global Biogeochemical Cycles, 20,

862   Gb2015, doi: 2010.1029/2005gb002532, 2006.

863 Knutti, R. and Hegerl, G. C.: The equilibrium sensitivity of the Earth's

864 temperature to radiation changes, Nature Geoscience, 1, 735-743, doi:

865 710.1038/ngeo1337, 2008.

866 Kostadinov, T. S., Siegel, D. A., and Maritorena, S.: Retrieval of the particle size

867 distribution from satellite ocean color observations, Journal of Geophysical

868 Research-Oceans, 114, C09015, doi: 09010.01029/02009jc005303, 2009.

869 Kuhlbrodt, T. and Gregory, J. M.: Ocean heat uptake and its consequences for the

870 magnitude of sea level rise and climate change, Geophysical Research Letters, 39,

871 L18608, doi:18610.11029/12012GL052952, 2012.

872 Laufkötter, C., Vogt, M., Gruber, N., Aita-Noguchi, M., Aumont, O., Bopp, L.,

873 Buitenhuis, E., Doney, S. C., Dunne, J., Hashioka, T., Hauck, J., Hirata, T., John, J.,

874 Le Quere, C., Lima, I. D., Nakano, H., Seferian, R., Totterdell, I., Vichi, M., and

875 Volker, C.: Drivers and uncertainties of future global marine primary production

876 in marine ecosystem models, Biogeosciences, 12, 6955-6984, doi: 6910.5194/bg-

877 6912-6955-2015, 2015.

878 Le Quere, C., Harrison, S. P., Prentice, I. C., Buitenhuis, E. T., Aumont, O., Bopp,

879 L., Claustre, H., Da Cunha, L. C., Geider, R., Giraud, X., Klaas, C., Kohfeld, K. E.,

880 Legendre, L., Manizza, M., Platt, T., Rivkin, R. B., Sathyendranath, S., Uitz, J.,

881 Watson, A. J., and Wolf-Gladrow, D.: Ecosystem dynamics based on plankton

882 functional types for global ocean biogeochemistry models, Global Change

883 Biology, 11, 2016-2040, 2005.

884 Leung, S., Cabré, A., and Marinov, I.: A latitudinally banded phytoplankton

885 response to 21st century climate change in the Southern Ocean across the CMIP5

886 model suite, Biogeosciences, 12, 5715-5734, doi: 5710.5194/bg-5712-5715-2015,

887 2015.

888 Liu, M., Rajagopalan, K., Chung, S. H., Jiang, X., Harrison, J., Nergui, T.,

889 Guenther, A., Miller, C., Reyes, J., Tague, C., Choate, J., Salathé, E. P., Stöckle, C.

890 O., and Adam, J. C.: What is the importance of climate model bias when
891 projecting the impacts of climate change on land surface processes?,
892 Biogeosciences, 11, 2601-2622, doi: 2610.5194/bg-2611-2601-2014, 2014.

893 Luo, Y. Y., Liu, Q. Y., and Rothstein, L. M.: Simulated response of North Pacific
894 Mode Waters to global warming, Geophysical Research Letters, 36, L23609, doi:
895 23610.21029/22009gl040906, 2009.

896 Lyman, J. M., Good, S. A., Gouretski, V. V., Ishii, M., Johnson, G. C., Palmer, M.
897 D., Smith, D. M., and Willis, J. K.: Robust warming of the global upper ocean,
898 Nature, 465, 334-337, 2010.

899 Manizza, M., Le Quere, C., Watson, A. J., and Buitenhuis, E. T.: Ocean
900 biogeochemical response to phytoplankton-light feedback in a global model,
901 Journal of Geophysical Research-Oceans, 113, C10010,
902 doi:10010.11029/12007jc004478, 2008.

903 Marinov, I., Doney, S. C., Lima, I. D., Lindsay, K., Moore, J. K., and Mahowald,
904 N.: North-South asymmetry in the modeled phytoplankton community response
905 to climate change over the 21st century, Global Biogeochemical Cycles, 27, 1274-
906 1290, doi: 1210.1002/2013gb004599, 2013.

907 Misumi, K., Lindsay, K., Moore, J., Doney, S., Bryan, F., Tsumune, D., and
908 Yoshida, Y.: The iron budget in ocean surface waters in the 20th and 21st
909 centuries: projections by the Community Earth System Model version 1,
910 Biogeosciences, 11, 33-55, doi: 10.5194/bg-5111-5133-2014, 2014.

911 Moore, J., Lindsay, K., Doney, S., Long, M., and Misumi, K.: Marine Ecosystem
912 Dynamics and Biogeochemical Cycling in the Community Earth System Model
913 [CESM1(BGC)]: Comparison of the 1990s with the 2090s under the RCP4.5 and
914 RCP8.5 Scenarios, J Climate, 26, 9291-9312, 2013.

915 Moss, R. H., Edmonds, J. A., Hibbard, K. A., Manning, M. R., Rose, S. K., van
916 Vuuren, D. P., Carter, T. R., Emori, S., Kainuma, M., Kram, T., Meehl, G. A.,

Mitchell, J. F. B., Nakicenovic, N., Riahi, K., Smith, S. J., Stouffer, R. J., Thomson, A. M., Weyant, J. P., and Wilbanks, T. J.: The next generation of scenarios for climate change research and assessment, Nature, 463, 747-756, 2010.

Passow, U. and Carlson, C. A.: The biological pump in a high CO2 world, Marine Ecology Progress Series, 470, 249-271, 2012.

Plattner, G. K., Joos, F., Stocker, T. F., and Marchal, O.: Feedback mechanisms and sensitivities of ocean carbon uptake under global warming, Tellus Series B-Chemical and Physical Meteorology, 53, 564-592, 2001.

Pollard, R. T., Salter, I., Sanders, R. J., Lucas, M. I., Moore, C. M., Mills, R. A., Statham, P. J., Allen, J. T., Baker, A. R., Bakker, D. C., Charette, M. A., Fielding, S., Fones, G. R., French, M., Hickman, A. E., Holland, R. J., Hughes, J. A., Jickells, T. D., Lampitt, R. S., Morris, P. J., Nedelec, F. H., Nielsdottir, M., Planquette, H., Popova, E. E., Poulton, A. J., Read, J. F., Seeyave, S., Smith, T., Stinchcombe, M., Taylor, S., Thomalla, S., Venables, H. J., Williamson, R., and Zubkov, M. V.: Southern Ocean deep-water carbon export enhanced by natural iron fertilization, Nature, 457, 577-581, 2009.

Pomeroy, L. R.: The ocean's food web, a changing paradigm, Bioscience, 24, 499-504, 1974.

Randerson, J. T., Lindsay, K., Munoz, E., Fu, W., Moore, J. K., Hoffman, F. M., Mahowald, N. M., and Doney, S. C.: Multicentury changes in ocean and land contributions to the climate-carbon feedback, Global Biogeochemical Cycles, 29, 744-759, doi: 710.1002/2014gb005079, 2015.

Schmittner, A., Oschlies, A., Matthews, H. D., and Galbraith, E. D.: Future changes in climate, ocean circulation, ecosystems, and biogeochemical cycling simulated for a business-as-usual CO2 emission scenario until year 4000 AD, Global Biogeochemical Cycles, 22, Gb1013, doi: 1010.1029/2007gb002953, 2008.

943 Schwinger, J., Tjiputra, J. F., Heinze, C., Bopp, L., Christian, J. R., Gehlen, M.,

944 Ilyina, T., Jones, C. D., Salas-Melia, D., Segschneider, J., Séférian, R., and

945 Totterdell, I.: Nonlinearity of Ocean Carbon Cycle Feedbacks in CMIP5 Earth

946 System Models, J Climate, 27, 3869-3888, 2014.

947 Seferian, R., Bopp, L., Gehlen, M., Orr, J. C., Ethe, C., Cadule, P., Aumont, O.,

948 Salas y Melia, D., Voldoire, A., and Madec, G.: Skill assessment of three earth

949 system models with common marine biogeochemistry, Climate Dynamics, 40,

950 2549-2573, doi: 2510.1007/s00382-00012-01362-00388, 2013.

951 Séférian, R., Gehlen, M., Bopp, L., Resplandy, L., Orr, J. C., Marti, O., Dunne, J. P.,

952 Christian, J. R., Doney, S. C., Ilyina, T., Lindsay, K., Halloran, P. R., Heinze, C.,

953 Segschneider, J., Tjiputra, J., Aumont, O., and Romanou, A.: Inconsistent

954 strategies to spin up models in CMIP5: implications for ocean biogeochemical

955 model performance assessment, Geoscientific Model Development, 9, 1827-1851,

956 doi: 1810.5194/gmd-1829-1827-2016, 2016.

957 Sherman, E., Moore, J. K., Primeau, F., and Tanouye, D.: Temperature influence

958 on phytoplankton community growth rates, Global Biogeochemical Cycles, 30,

959 550-559, doi: 510.1002/2015GB005272, 2016.

960 Siegel, D. A., Buesseler, K. O., Doney, S. C., Sailley, S. F., Behrenfeld, M. J., and

961 Boyd, P. W.: Global assessment of ocean carbon export by combining satellite

962 observations and food-web models, Global Biogeochemical Cycles, 28, 181-196,

963 doi: 110.1002/2013gb004743, 2014.

964 Siegenthaler, U. and Wenk, T.: Rapid Atmospheric Co2 Variations And Ocean

965 Circulation, Nature, 308, 624-626, 1984.

966 Steinacher, M., Joos, F., Froelicher, T. L., Plattner, G. K., and Doney, S. C.:

967 Imminent ocean acidification in the Arctic projected with the NCAR global

968 coupled carbon cycle-climate model, Biogeosciences, 6, 515-533, doi: 510.5194/bg-

969 5196-5515-2009, 2009.

39

970 Steinacher, M., Joos, F., Frolicher, T. L., Bopp, L., Cadule, P., Cocco, V., Doney, S.

971 C., Gehlen, M., Lindsay, K., Moore, J. K., Schneider, B., and Segschneider, J.:

972 Projected 21st century decrease in marine productivity: a multi-model analysis,

973 Biogeosciences, 7, 979-1005, doi: 1010.5194/bg-1007-1979-2010, 2010.

974 Swart, N. C. and Fyfe, J. C.: Observed and simulated changes in the Southern

975 Hemisphere surface westerly wind-stress, Geophysical Research Letters, 39,

976 L16711, doi:16710.11029/12012GL052810, 2012.

977 Szopa, S., Balkanski, Y., Schulz, M., Bekki, S., Cugnet, D., Fortems-Cheiney, A.,

978 Turquety, S., Cozic, A., Deandreis, C., Hauglustaine, D., Idelkadi, A., Lathiere, J.,

979 Lefevre, F., Marchand, M., Vuolo, R., Yan, N., and Dufresne, J. L.: Aerosol and

980 ozone changes as forcing for climate evolution between 1850 and 2100, Climate

981 Dynamics, 40, 2223-2250, doi 2210.1007/S00382-00012-01408-Y, 2013.

982 Taylor, K. E., Stouffer, R. J., and Meehl, G. A.: An Overview Of Cmip5 And The

983 Experiment Design, Bulletin of the American Meteorological Society, 93, 485-498,

984 2012.

985 Tjiputra, J. F., Roelandt, C., Bentsen, M., Lawrence, D. M., Lorentzen, T.,

986 Schwinger, J., Seland, O., and Heinze, C.: Evaluation of the carbon cycle

987 components in the Norwegian Earth System Model (NorESM), Geoscientific

988 Model Development, 6, 301-325, doi: 310.5194/gmd-5196-5301-2013, 2013.

989 van Vuuren, D. P., Edmonds, J., Kainuma, M., Riahi, K., Thomson, A., Hibbard,

990 K., Hurtt, G. C., Kram, T., Krey, V., Lamarque, J.-F., Masui, T., Meinshausen, M.,

991 Nakicenovic, N., Smith, S. J., and Rose, S. K.: The representative concentration

992 pathways: an overview, Climatic Change, 109, 5-31, 2011.

993 Vancoppenolle, M., Bopp, L., Madec, G., Dunne, J., Ilyina, T., Halloran, P. R., and

994 Steiner, N.: Future Arctic Ocean primary productivity from CMIP5 simulations:

995 Uncertain outcome, but consistent mechanisms, Global Biogeochemical Cycles,

996 27, 605-619, doi: 610.1002/gbc.20055, 2013.

997 Vichi, M., Manzini, E., Fogli, P. G., Alessandri, A., Patara, L., Scoccimarro, E.,

998 Masina, S., and Navarra, A.: Global and regional ocean carbon uptake and

999 climate change: sensitivity to a substantial mitigation scenario, Climate

1000 Dynamics, 37, 1929-1947, doi: 1910.1007/s00382-00011-01079-00380, 2011.

1001

Figure 1. Time series of global mean surface stratification, SST and SSS for historical run and RCP8.5 over 1850-2100. Surface stratification is defined as the density difference between 200m and the surface. Red square indicates observations from the WOA2009 data.

Figure 2. The spatial pattern is shown for changes in stratification between the 1990s and the 2090s.

Figure 3. Time series of nitrate (NO_3), phosphate (PO_4), silicate (SiO_4) and dissolved iron (dFe) concentrations (0-100 m) are shown for 1850-2100. Red square indicates WOA2009 global mean values.

Figure 4. Time series are displayed of mean changes (in percent) relative to the 1990s for (a) NO_3, (b) PO_4, (c) SiO_4 and (d) dFe (0-100m) during 1850-2100.

Figure 5. Time series of global mean net primary production, export production, and the particle export ratio over 1850-2100 are shown for each model.

Figure 6. Time series are displayed of the percent changes in net primary production, export production, and the particle export ratio, and stratification over the period 1850-2100 (each relative to their 1990s means).

Figure 7. Relationships are shown between the relative percent change in surface stratification with climate and the relative change in several biogeochemical variables including net primary production (NPP) (a), silicate (b), nitrate (c), phosphate (d), export production (EP) (e), the fraction of NPP by diatoms (g). EP is plotted against the change in the fraction of NPP by diatoms (g) and against the change in NPP (h). All changes are relative to the 1990s and plotted over 1850-2100. These time series are derived from global annual mean data.

Figure 8. The fraction of total NPP by diatoms for the 1990s is shown for each model (data for NorESM not available).

Figure 9. The percent change in NPP by diatoms between the 2090s and the 1990s.

Figure 10. The mean particle export ratio (pe-ratio) for the 1990s is shown for each model.

Figure 11. The percent change in the particle export ratio (pe-ratio) between the 2090s and the 1990s).

Figure 12. The stratification bias for the 1990s is plotted for each model versus the relative changes in NPP (a), EP (b), and stratification (c) with climate change (2090s – 1990s). All three linear regressions are statistically significant at a level >95%.

Supplementary Figure Captions

Figure S1. Mean vertical profiles are shown for density (a), temperature (c) and salinity (e) for the 1990s. Changes between the 2090s-1990s are shown in (b), (d) and (f), for the same variables. Solid black line denotes WOA2009 data.

Figure S2. Fractional contribution of temperature to the stratification change from the 1990s to the 2090s is shown for each model.

Figure S3. Mean NO_3 concentrations in the first 100 m for the1990s, the modeling efficiency (MEF) (Stow et al., 2009) and logarithmic transformed root mean square error (RMSE) are indicated relative to observations from the WOA2009.

Supplementary References:
Stow, C. A., Jolliff, J., McGillicuddy, D. J., Doney, S. C., Allen, J. I., Friedrichs, M. A. M., Rose, K. A., and Wallheadg, P.: Skill assessment for coupled biological/physical models of marine systems, Journal of Marine Systems, 76, 4-15, 2009.

Table 1: A brief description of components of the ESMs used in this study, for atmosphere and ocean components, the number of levels in the vertical is indicated by 'lev' and then the horizontal resolution is indicated in degrees, vertical coordinates of the ocean and biogeochemical components are indicated by Z (geopotential) or I (isopycnal).

Model	Resolution		Vertical coordinate	Reference	Biogeochemical component	References
	Atmosphere	Ocean				
GFDL-ES2M	24 lev,2.5/2.0°	50 lev,0,3-1°	Z	Dunne et al. (2013a)	TOPAZ2	Dunne et al. (2013b)
GFDL-ES2G	24 lev,2.5/2.0°	50 lev,0,3-1°	Z+I	Dunne et al. (2013a)	TOPAZ2	Dunne et al. (2013b)
MPI-ESM-LR	47 lev,1.9°	40 lev, 1.5°	Z	Giorgetta et al. (2013)	HAMOCC5.2	Ilyina et al. (2013)
MPI-ESM-MR	47 lev,1.9°	40 lev, 0.4°	Z	Giorgetta et al. (2013)	HAMOCC5.2	Ilyina et al. (2013)
IPSL-CM5A-LR	39 lev,1.9/3.8°	31 lev, 0.5-2°	Z	Dufresne et al. (2013)	PISCES	Aumont and Bopp (2006)
IPSL-CM5A-MR	39 lev,1.2/1.9°	31 lev, 0.5-2°	Z	Dufresne et al. (2013)	PISCES	Aumont and Bopp (2006)
						Seferian et al (2013)
HadGEM2-ES	38 lev,1.2/1.9°	40 lev, 0.3-1°	Z	Jones et al (2011)	Diat-HadOCC	Palmer and Totterdell (2000)
				Collins et al. (2011)		
CESM1(BGC)	26 lev,1.25/0.94°	60 lev, 1.125°	Z	Gent et al. (2011)	BEC	Moore et al. (2004)
		/0.27-0.53°		Lindsay et al. (2013)		Doney et al (2009)
NorESM1-ME	26 lev,1.9°	70 lev, 1.5°	I	Bentsen et al. (2013)	HAMOCC5.1	Tjiputra et al. (2013)

Table 2: A brief description of the marine biogeochemical components included in the ESMs. Nutrients limiting phytoplankton growth, the number of explicit phytoplankton groups, the number of explicit zooplankton groups, representation of heterotrophic bacteria, the use of fixed fixed (Redfield: R) or variable (V) ratios for organic matter production, and Q_{10} for temperature dependency of biogeochemical processes (autotrophic/heterotrophic) are indicated.

Model	Nutrients	Phytoplankton	Zooplankton	Organic Materia Ratio	Q_{10}
TOPAZ2	5 ($NO_3, NH_4, PO_4,$ SiO_4, F_e)	3 (diatom, eukaryotes, small diazotrophs)	1	R(C:N) V(P, S_i, Chl, F_e)	1.88
HAMOCC5.2	3 (NO_3, F_e, PO_4)	1 (separated into, diatoms and calcifiers)	1	R(C:N:P:Fe)	1.88
HAMOCC5.1	3 (NO_3, F_e, PO_4)	1 (separated into, diatoms and calcifiers)	1	R(C:N:P:Fe)	1.88
PISCES	5 ($NO_3, F_e, PO_4,$ NH_4, SiO_4)	2 (diatoms and, nanophytoplankton)	2 (micro and meso-)	R(C:N:P) V(S_i, Chl, F_e)	1.88/2.14
Diat-HadOCC	4 ($NO_3, F_e,$ NH_4, SiO_4)	2 (diatoms and, non-diatom)	1	R(C:N) V(S_i, F_e)	none
BEC	5 ($NO_3, NH_4, PO_4,$ SiO_4, F_e)	3 (diatom, nano-, phyto, diazotrophy)	1	R(C:N:P) V(S_i, Chl, F_e)	2.0

Table 3: Global average of sea surface temperature (SST), sea surface salinity (SSS), nitrate (NO_3), phosphate(PO_4), NPP, EP, particle export ratio (pe-ratio), stratification index (SI) defined as density difference between 200 m and the surface and NPP by diatom (%) for the 1990s and 2090s. Observed estimates for the 1990s are obtained from WOA09 data for SST, SSS, nitrate and phosphate, from Carr et al. (2006) for NPP.

	SST °C		SSS psu		NO3(0-100m) mmol/m³		PO4(0-100m) mmol/m³		NPP PgC/yr		EP PgC/yr		pe-ratio %		SI kg/m³		%Diat %	
	1990s	2090s	1990s	2090s	1990s	2090s	1990s	2090s	1990s	2090s	1990s	2090s	1990s	2090s	1990s	2090s	1990s	2090s
Observations	18.3		34.57		6.73		0.63		50.0						1.81			
GFDL-ESM2G	18.5	20.4	34.06	33.98	6.65	6.10	0.66	0.58	57.8	57.5	4.40	4.10	7.60	7.02	2.35	2.75	10.7	9.7
GFDL-ESM2M	18.8	20.6	34.32	34.24	8.67	8.22	0.58	0.55	77.6	78.1	6.54	6.06	8.44	7.77	1.95	2.31	9.4	8.8
MPI-ESM-LR	18.3	20.7	34.38	34.23	7.20	6.61	0.57	0.50	45.7	41.6	7.23	6.05	15.84	14.56	1.88	2.41	78.7	80.1
MPI-ESM-MR	18.4	20.9	34.41	34.25	6.96	6.45	0.53	0.47	47.9	43.0	6.56	5.67	13.70	13.20	1.97	2.50	91.1	92.2
IPSL-CM5A-LR	17.7	21.0	34.52	34.43	5.62	4.81	0.43	0.36	28.9	27.0	5.96	4.87	20.61	18.05	2.05	2.63	23.1	20.3
IPSL-CM5A-MR	18.2	21.5	34.42	34.33	5.82	4.99	0.45	0.38	31.8	29.3	6.33	5.28	19.94	17.99	2.12	2.75	22.0	19.7
HadGEM2-ES	18.3	21.5	34.06	33.83	6.56	5.82	0.44	0.36	34.5	29.7	4.77	4.10	13.82	13.79	2.45	3.18	58.8	58.3
CESM1(BGC)	19.0	21.4	34.23	34.18	7.60	6.56	0.71	0.54	54.2	52.1	6.97	6.26	12.86	12.03	2.25	2.63	35.7	33.2
NorESM1-ME	18.1	20.2	34.34	34.26	7.01	6.18	0.60	0.51	38.6	35.3	6.81	6.18	17.64	17.52	1.74	2.01		
Model Mean	18.4	20.9	34.30	34.19	6.90	6.19	0.55	0.47	46.3	43.7	6.17	5.39	14.49	13.55	2.08	2.57	41.2	40.3
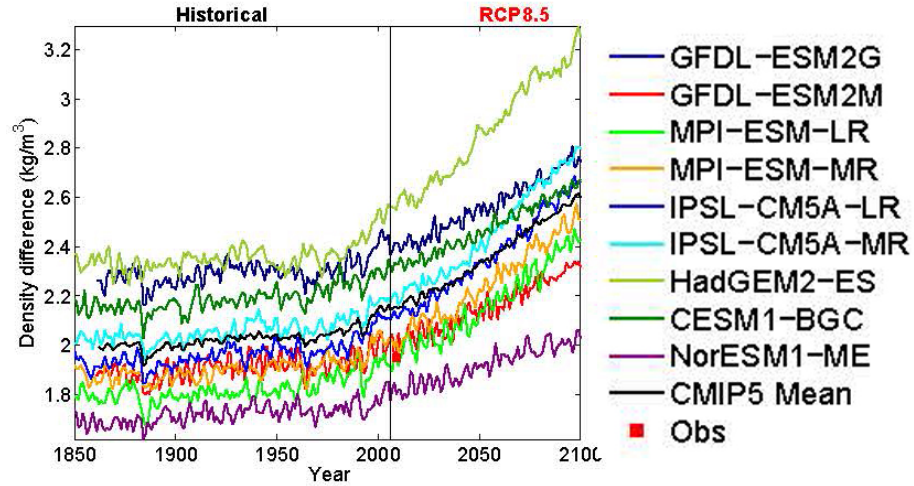
(a) Stratification
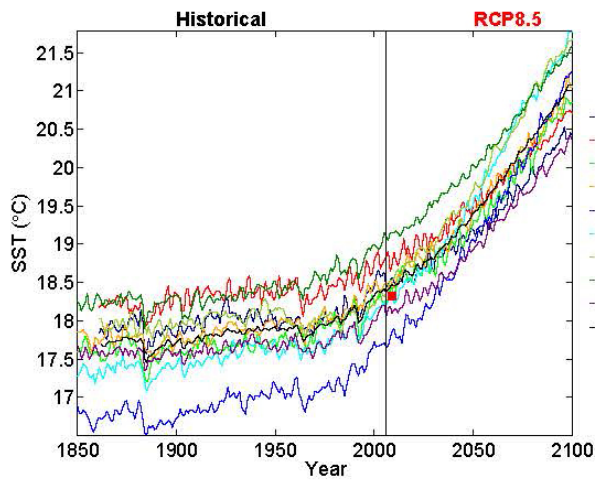
(b) SST
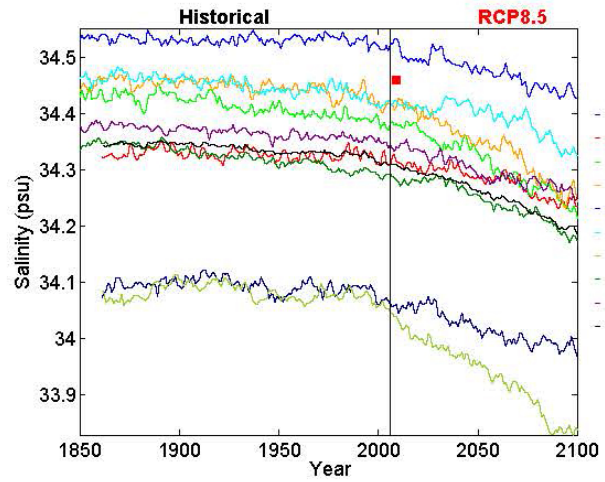
(c) SSS

Fig. 1: Time series of global mean stratification, SST and SSS for historical run and RCP8.5 over 1850-2100. Stratification is defined as the density difference between 200 m and the surface. Red square indicates observations from the WOA2009 data.
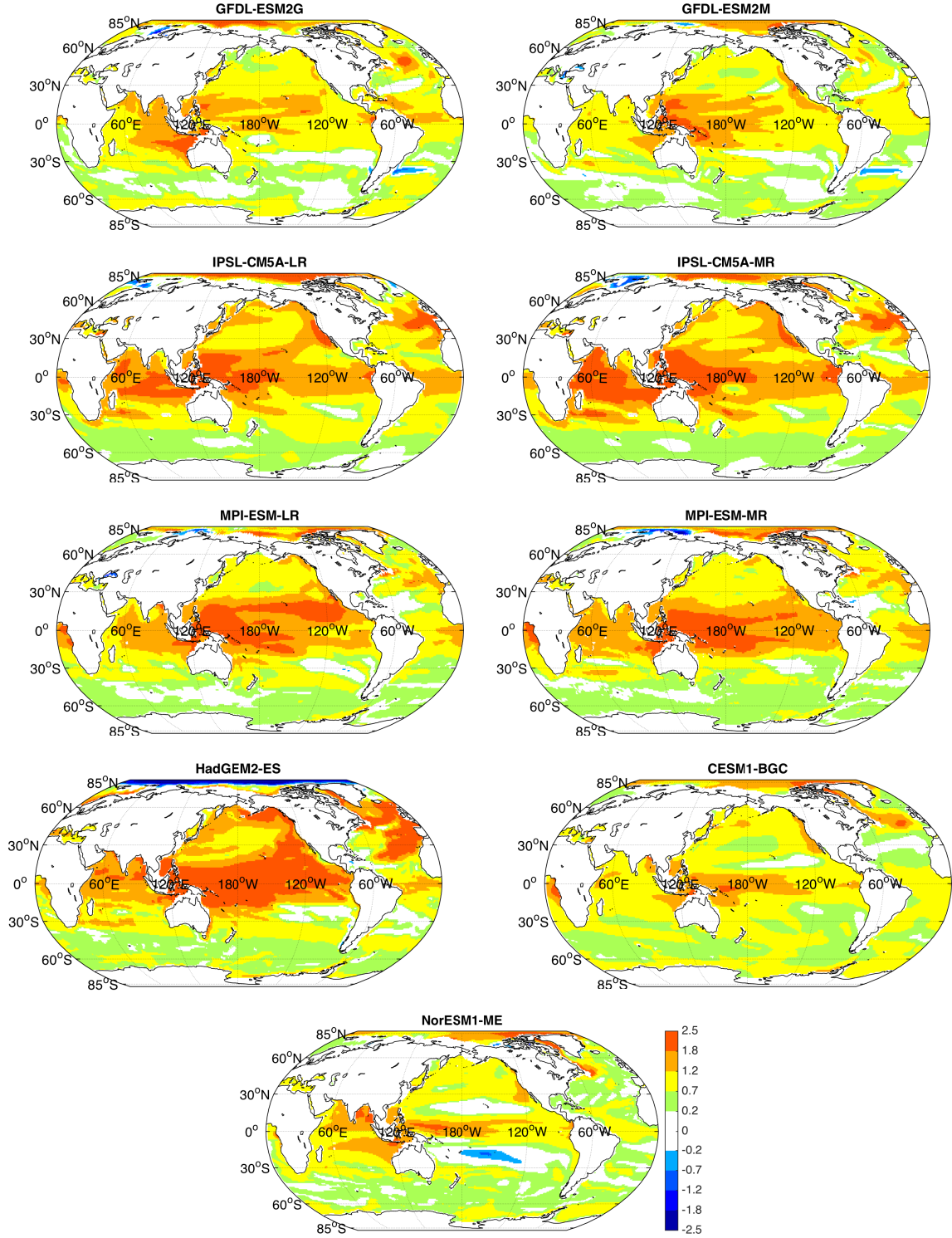
47

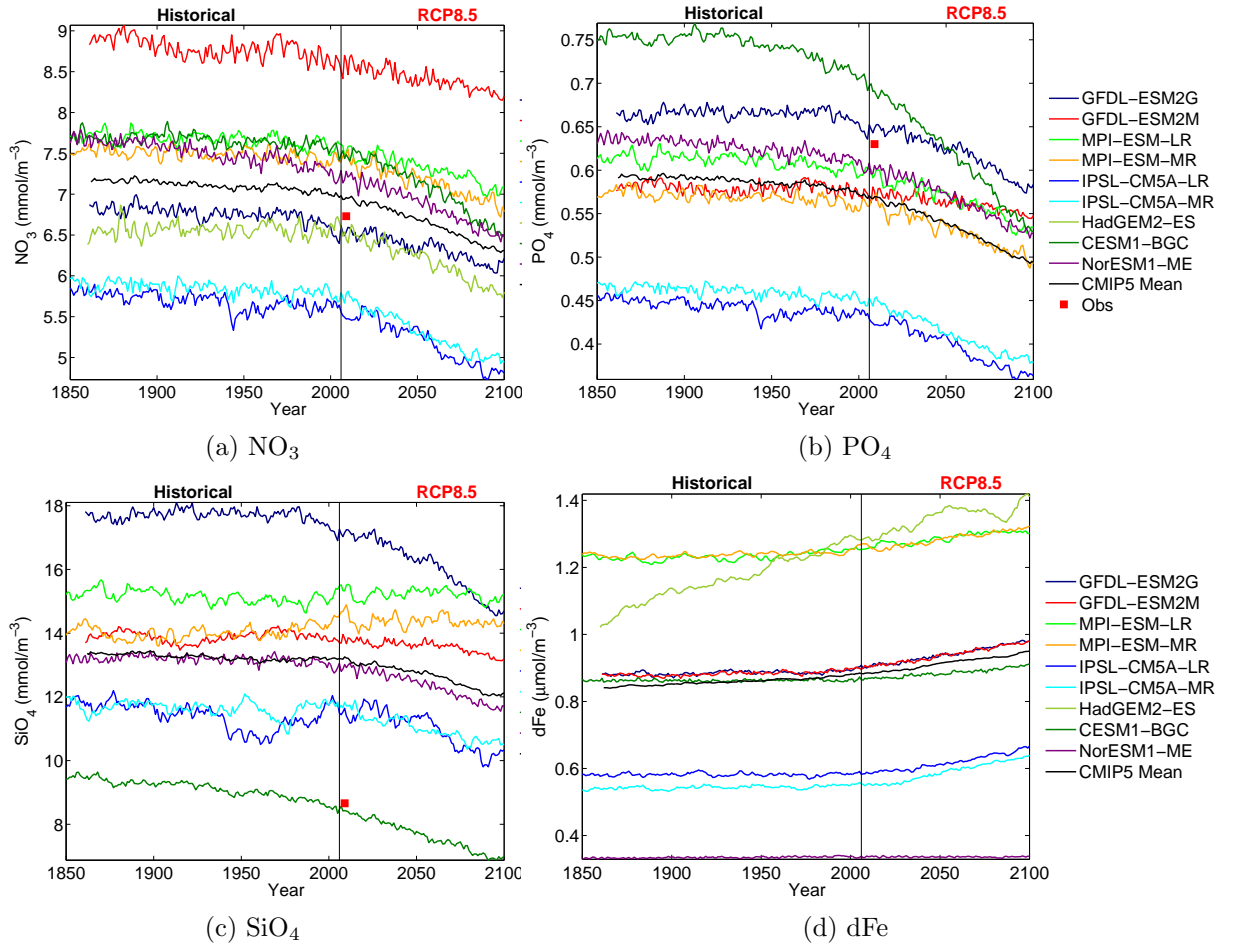Fig. 2: The spatial pattern is shown for changes in stratification between the 1990s and the 2090s.

(a) NO$_3$

(b) PO$_4$

(c) SiO$_4$

(d) dFe

Fig. 3: Time series of mean nitrate (NO$_3$), phosphate (PO$_4$), silicate (SiO$_4$) and dissolved iron (dFe) concentrations (0-100 m) are shown for 1850-2100. Red square indicates WOA2009 global mean values.

(a) NO3 change

(b) PO4 change

(c) SiO4 change

(d) dFe change
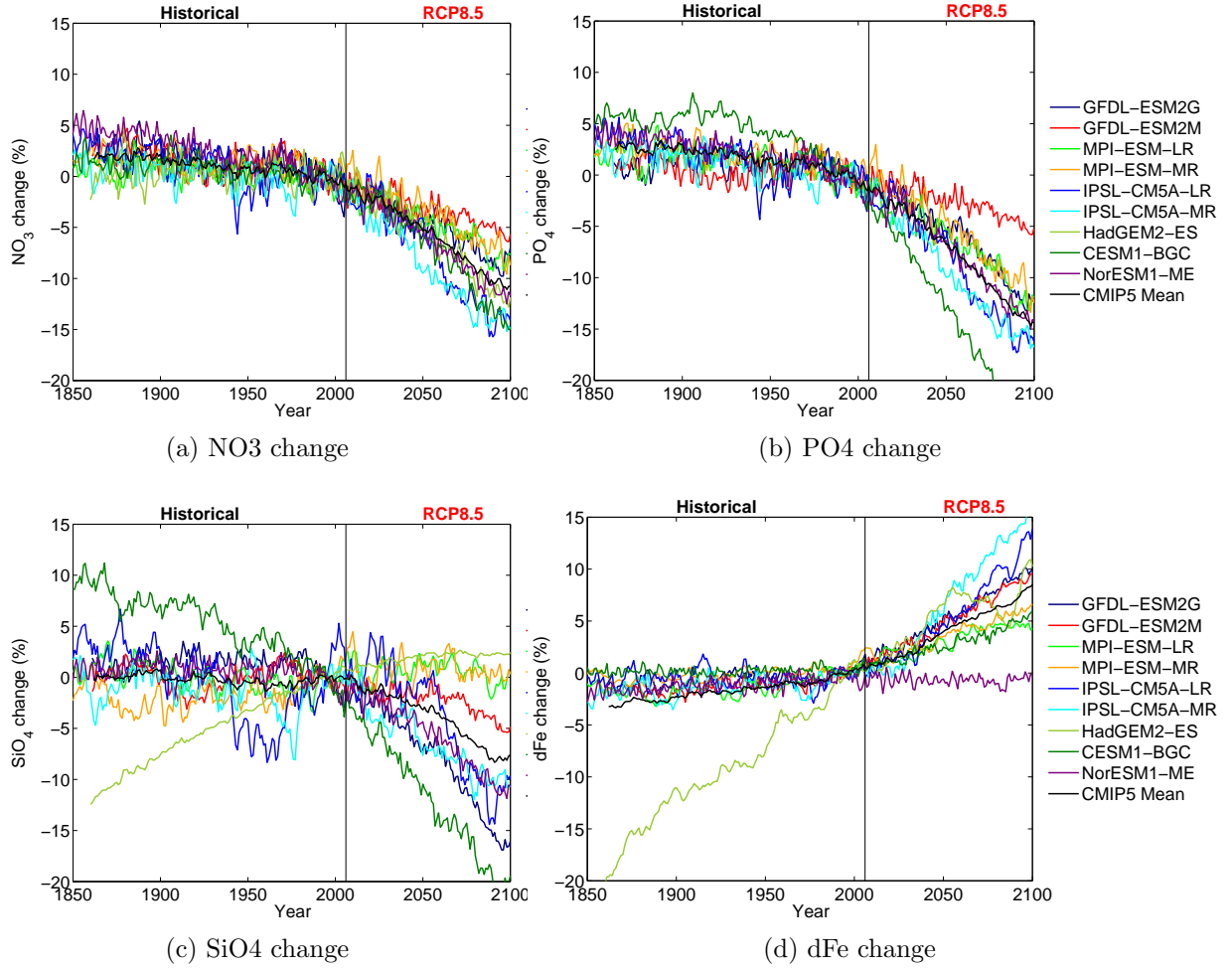
Fig. 4: Time series are displayed of mean changes (%) relative to the 1990s for (a)NO$_3$, (b)PO$_4$, (c)SiO$_4$ and (d) dFe (0-100m) during 1850-2100.

(a) NPP

(b) EP
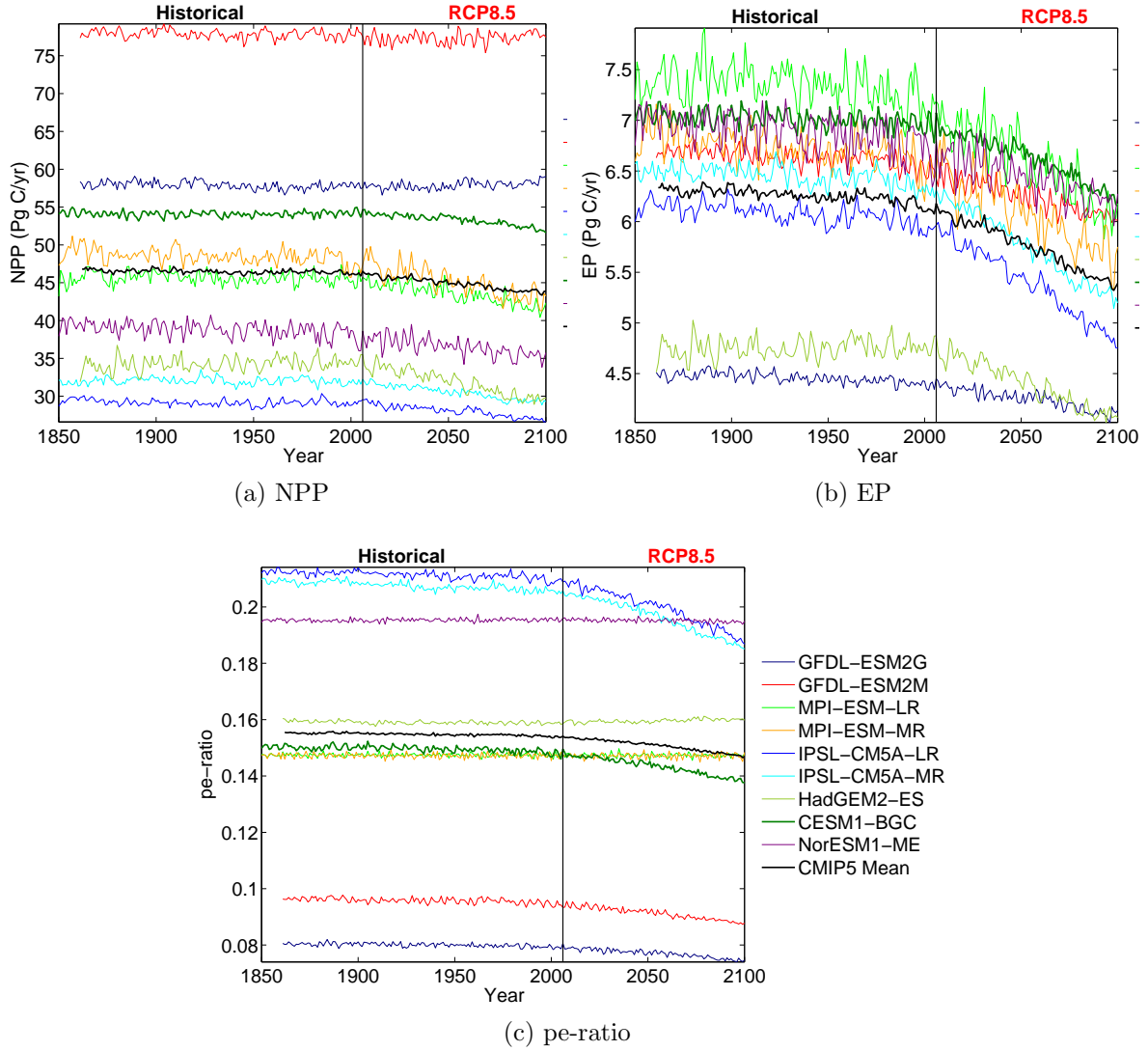
(c) pe-ratio

Fig. 5: Time series of global mean NPP, EP, and pe-ratio over 1850-2100 are shown for each model.

(a) NPP change

(b) EP change

(c) SI change
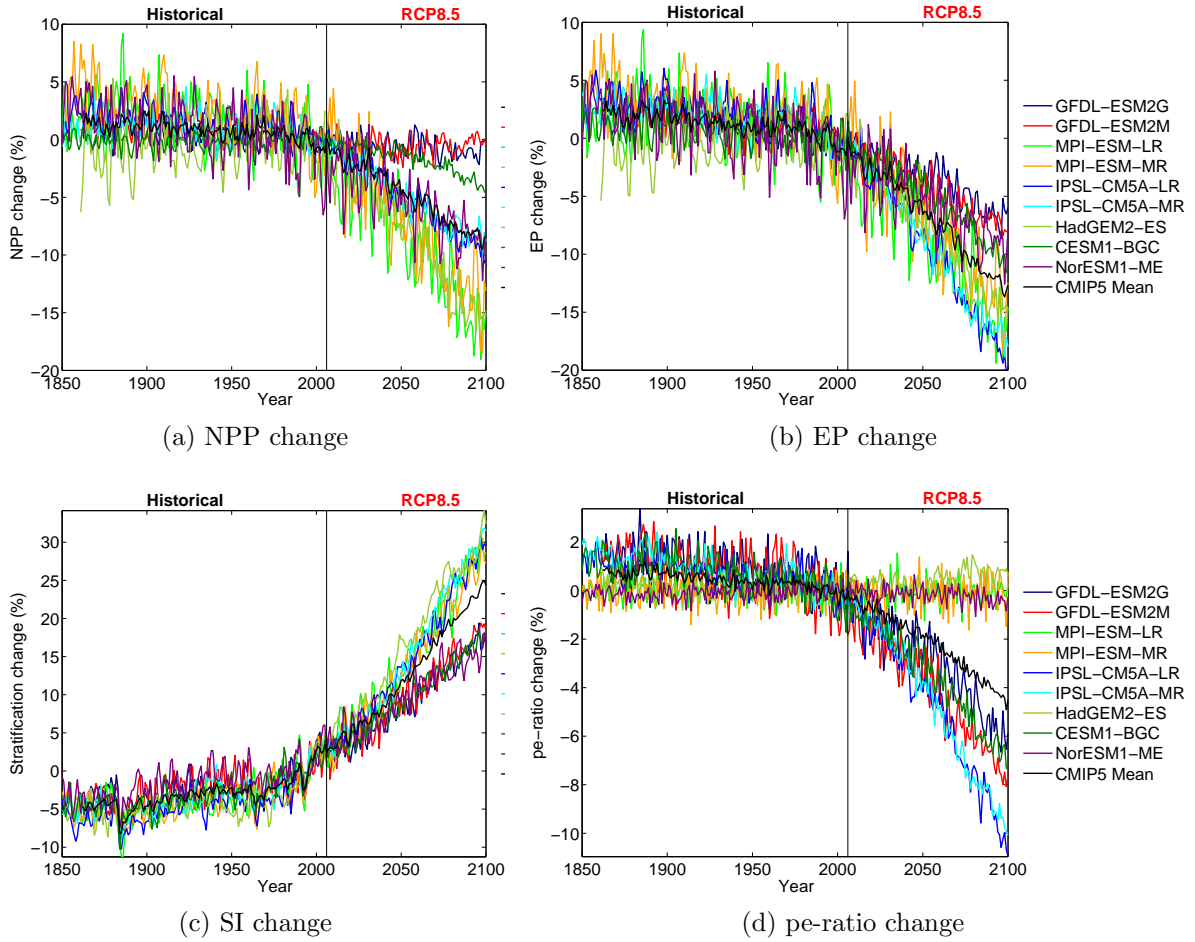
(d) pe-ratio change

Fig. 6: Time series are displayed of the percent changes in NPP, EP, pe-ratio and stratification over the period 1850-2100 (each relative to the 1990s means).

(a) ΔSI vs ΔNPP

(b) ΔSI vs ΔSiO$_4$

(c) ΔSI vs ΔNO$_3$

(d) ΔSI vs ΔPO$_4$

(e) ΔSI vs ΔEP

(f) ΔSI vs ΔNPP by diatom

(g) ΔNPP by diatom vs ΔEP

(h) ΔNPP vs ΔEP
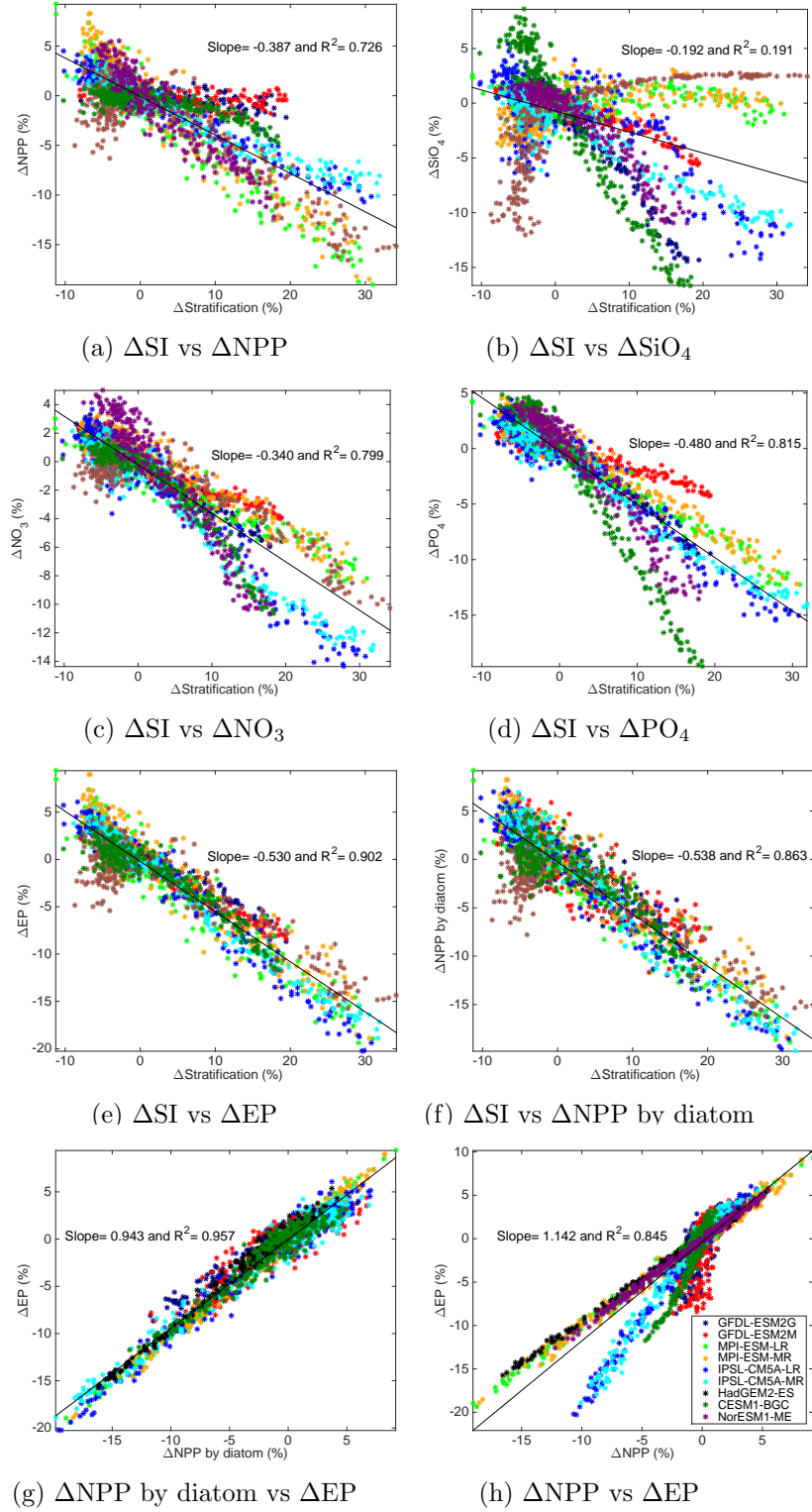
Fig. 7: Relationship are shown between the relative percent change in the stratification index (SI) with climate and the relative changes in several biogeochemical variables including NPP (a), silicate (b), nitrate (c), phosphate (d), EP (e), the fraction of NPP by diatoms (f). EP is plotted against the change in the fraction of NPP by diatoms (g) and against the change in NPP (h). All changes are relative to the 1990s and plotted over 1850-2100. Results are derived from global annual mean data .

53
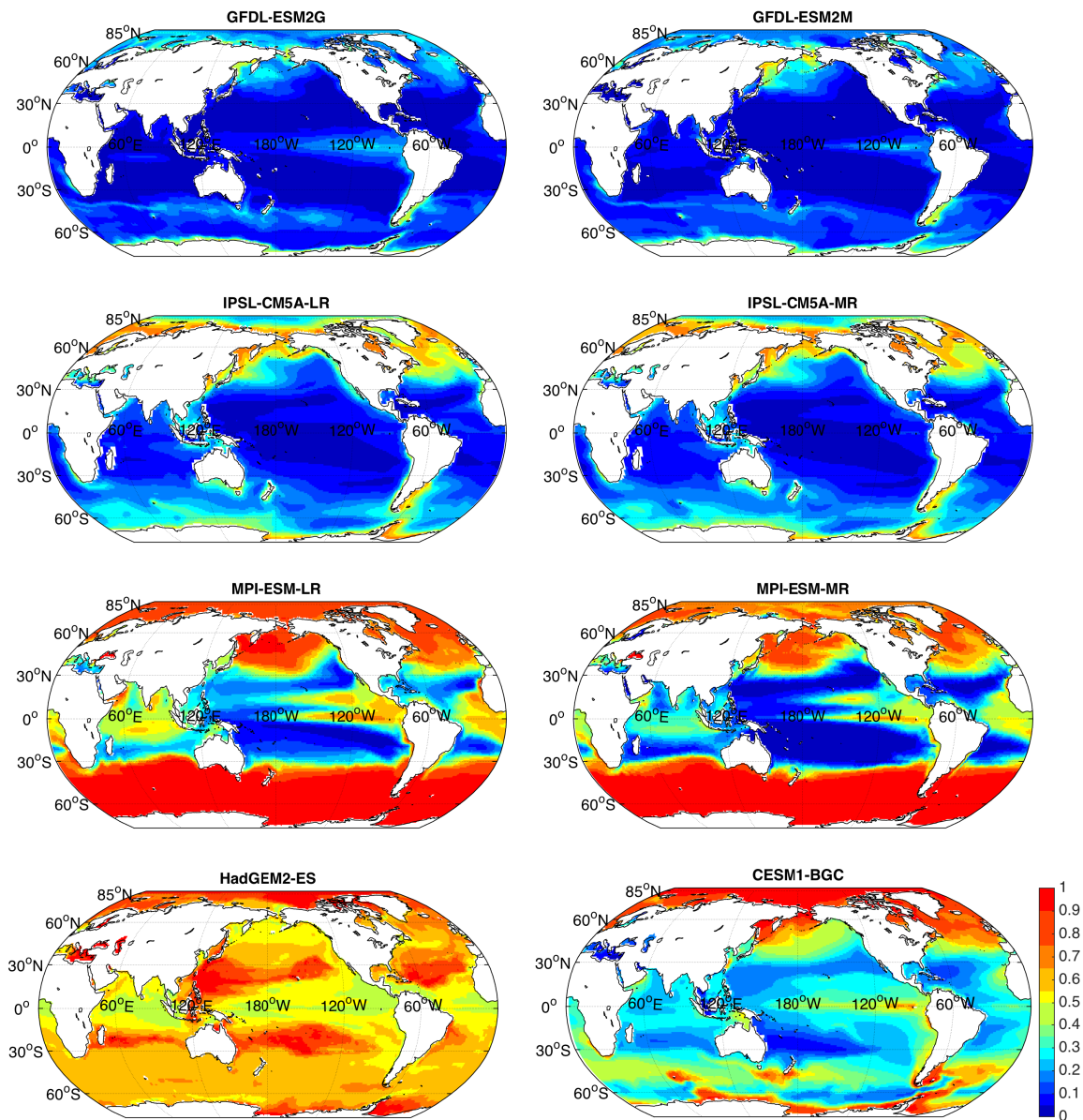
Fig. 8: The fraction of total NPP by the diatom for the 1990s is shown for each model (data for NorESM not available).
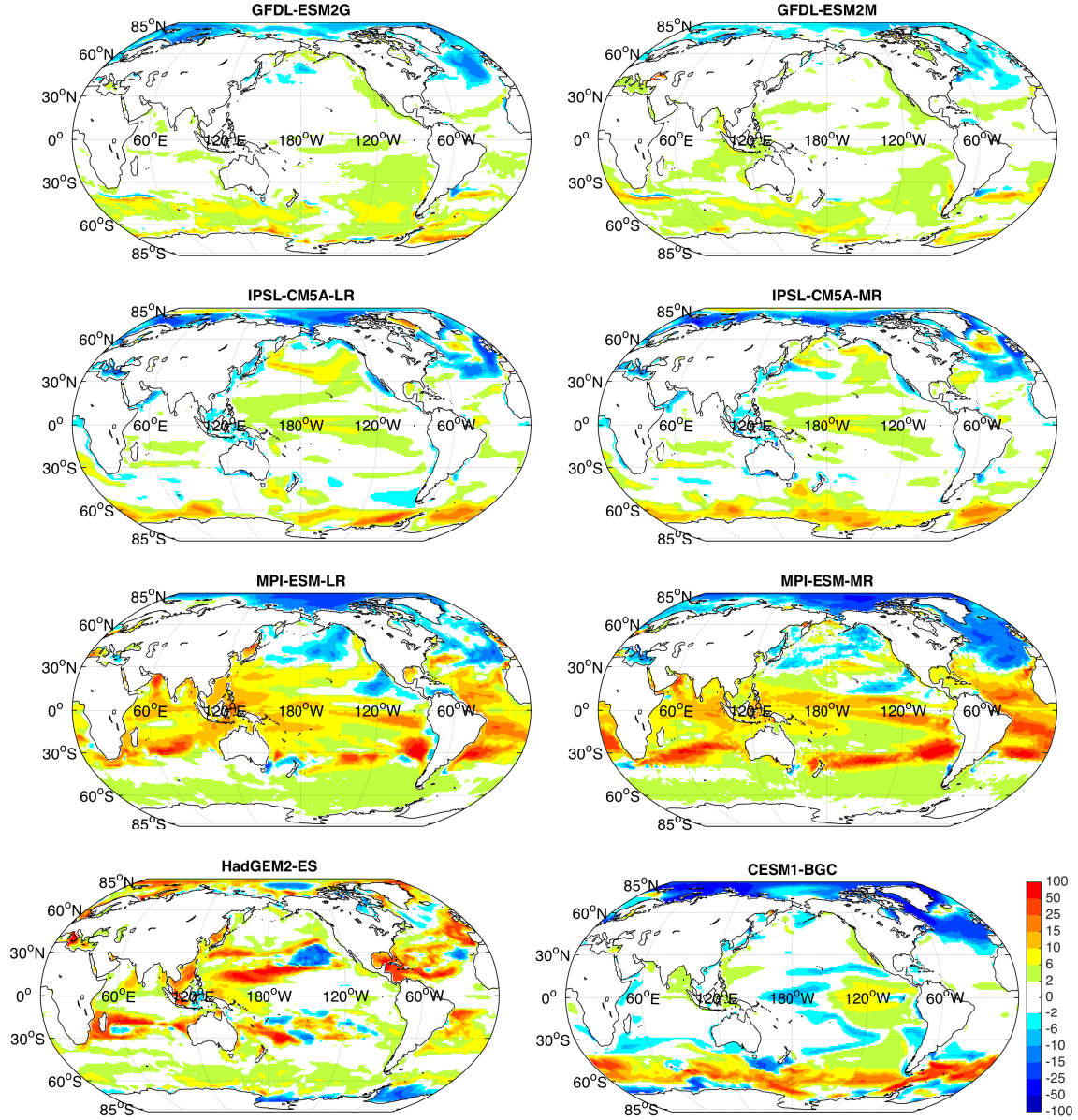
Fig. 9: The percent change in total NPP by diatoms between the 2090s and the 1990s.
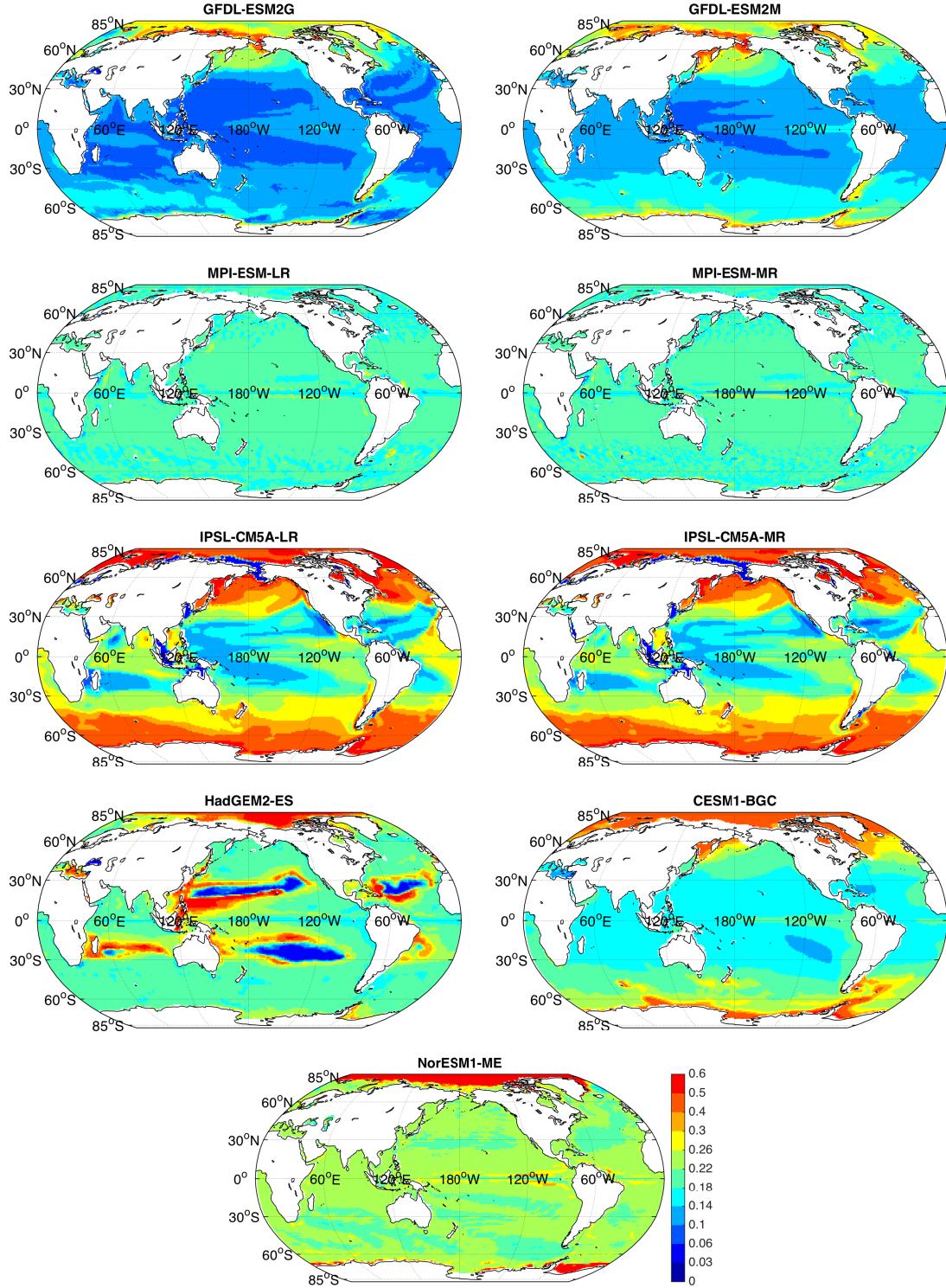
Fig. 10: The mean particle export ratio (pe-ratio) for the 1990s is shown for each model.
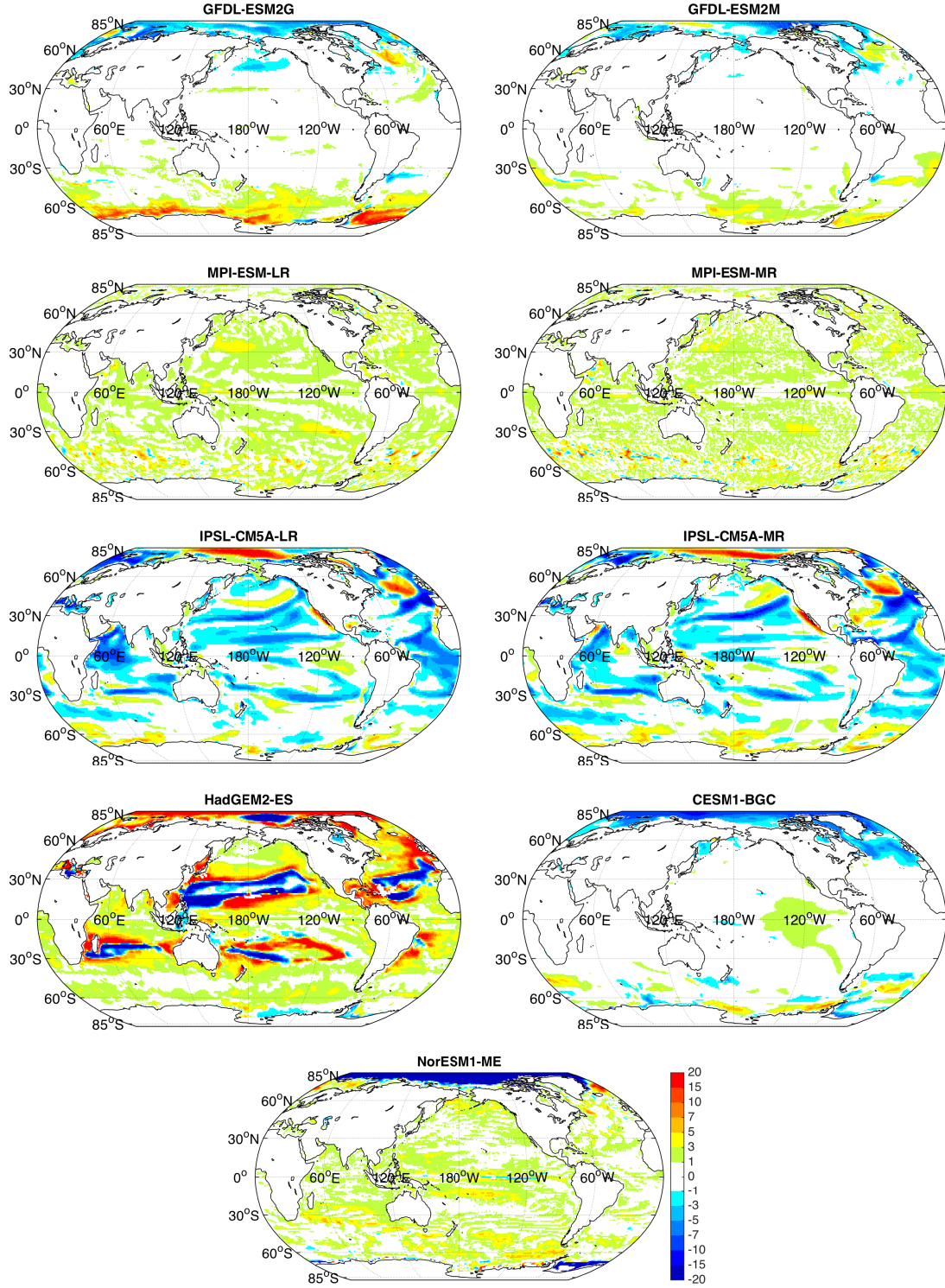
Fig. 11: The percent change in particle export ratio (pe-ratio) between the 2090s and the 1990s.
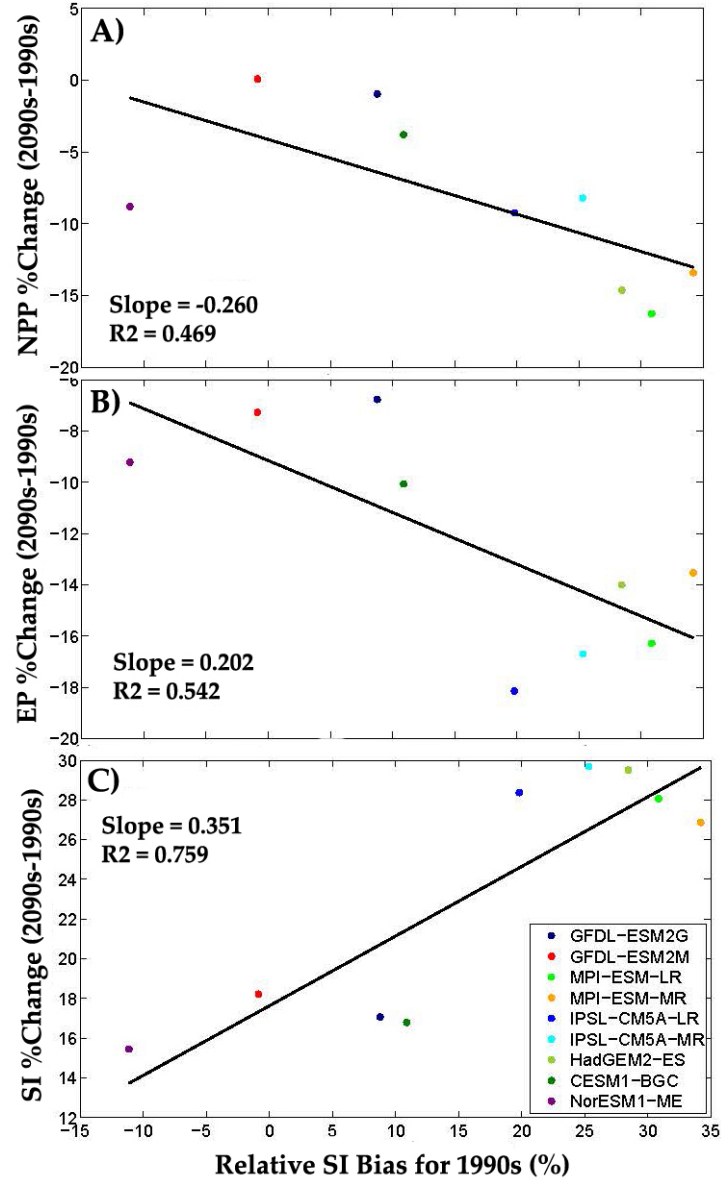
Fig. 12: The stratification bias for the 1990s is plotted for each model versus the relative changes in NPP (a), EP (b), and pe-ratio (c) with climate change (2090s-1990s). All three linear regressions are statistically significant at a level >95% .

(a) density profile

(b) density change

(c) temperature profile

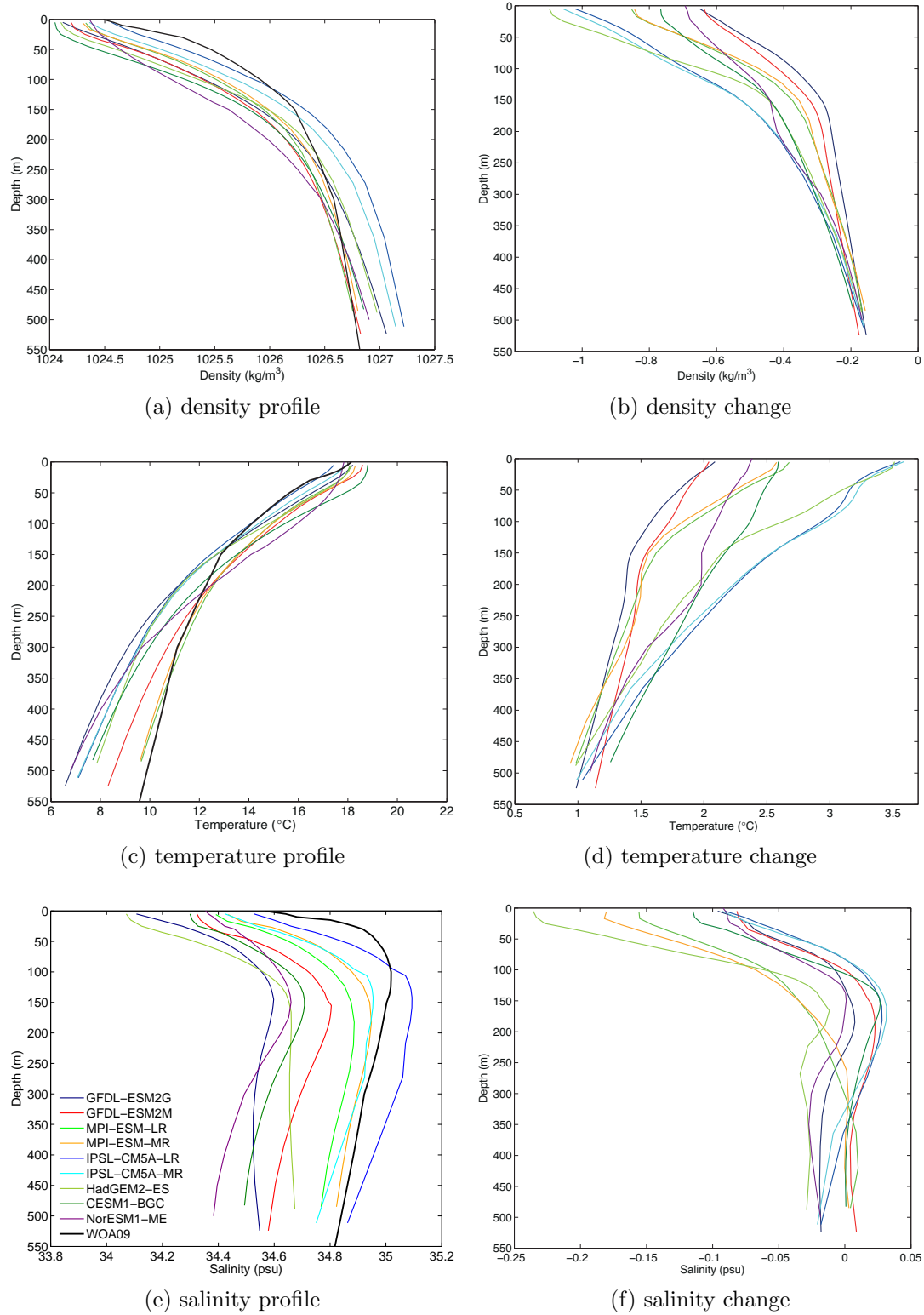(d) temperature change

(e) salinity profile

(f) salinity change

Figure S1. Mean vertical profiles are shown for density (a), temperature (c) and salinity (e) for the 1990s. Changes between the 2090s and1990s are shown in (b), (d) and (f), for the same variables. Solid black line denotes WOA2009 data.
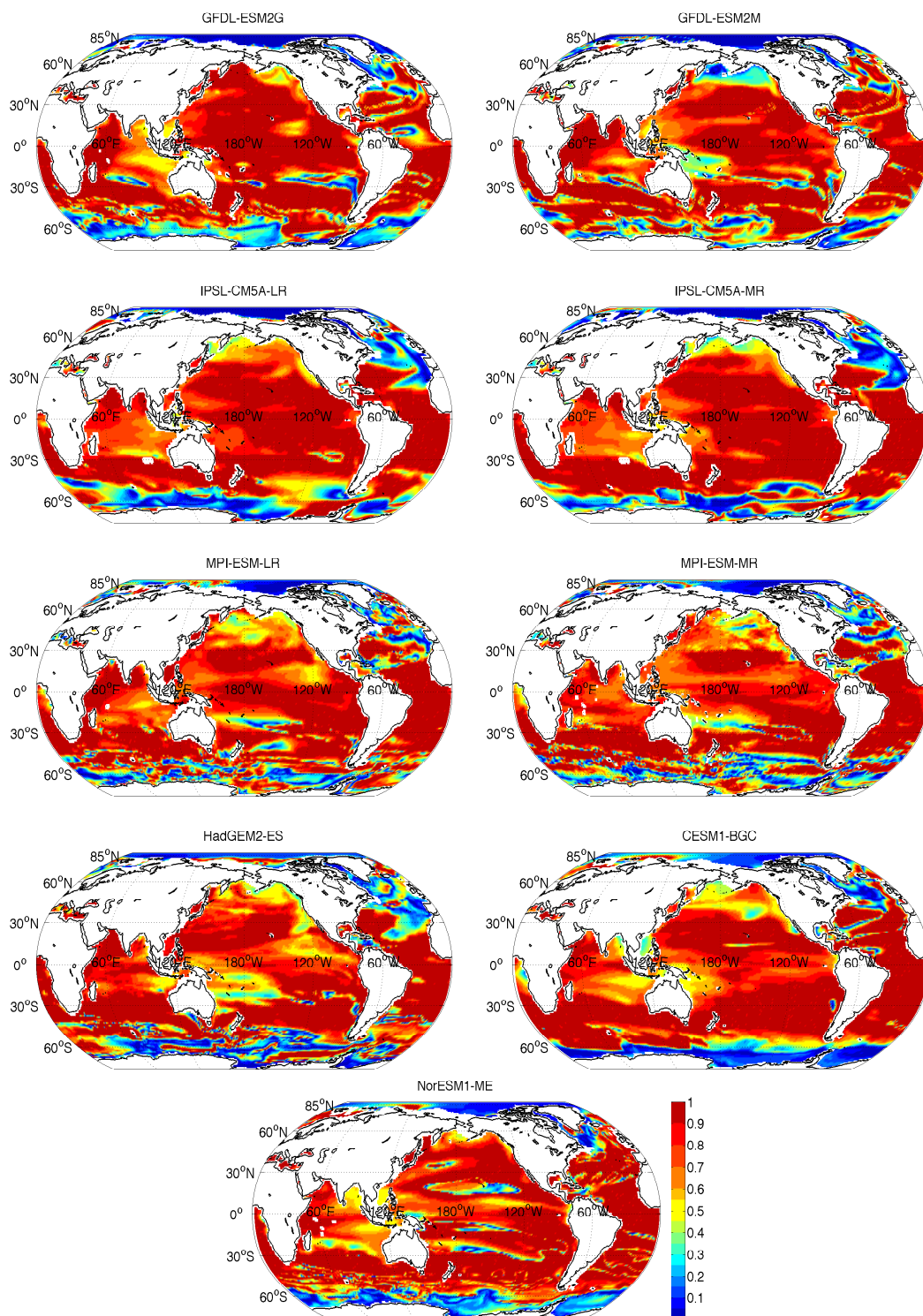
59

Figure S2. Fractional contribution of temperature to the stratification change from the 1990s to the 2090s is shown for each model.

GFDL-ESM2G

MEF = 0.873 RMSE(log) = 0.48mmol/m^3

GFDL-ESM2M

MEF = 0.796 RMSE(log) = 0.6mmol/m^3

IPSL-CM5A-LR

MEF = 0.844 RMSE(log) = 0.54mmol/m^3

IPSL-CM5A-MR

MEF = 0.873 RMSE(log) = 0.48mmol/m^3

MPI-ESM-LR

MEF = 0.827 RMSE(log) = 0.57mmol/m^3

MPI-ESM-MR

MEF = 0.809 RMSE(log) = 0.6mmol/m^3

HadGEM2-ES

MEF = 0.870 RMSE(log) = 0.51mmol/m^3

CESM1-BGC

MEF = 0.873 RMSE(log) = 0.92mmol/m^3

NorESM1-ME

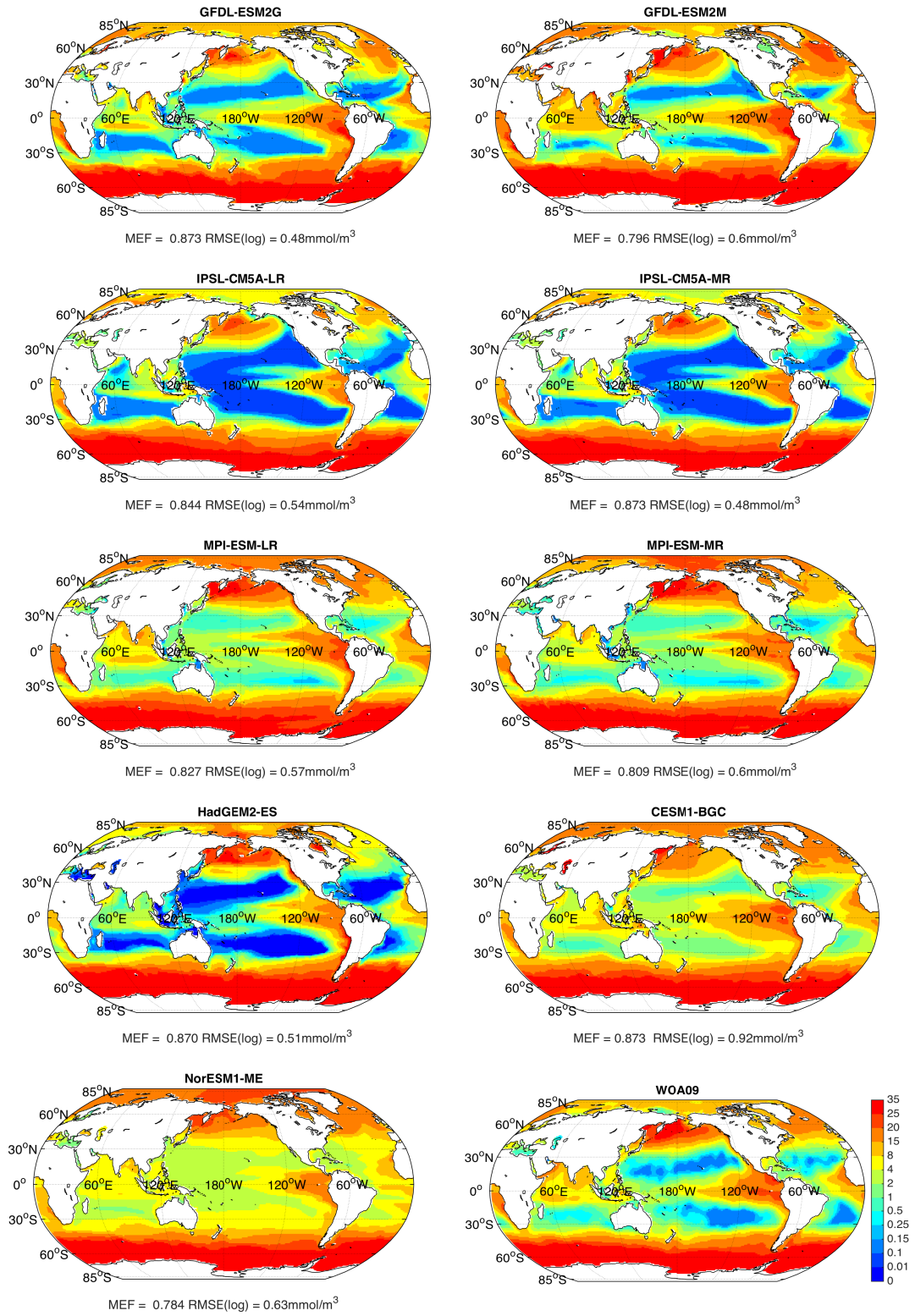MEF = 0.784 RMSE(log) = 0.63mmol/m^3

WOA09

Figure S3. Mean nitrate concentrations in the first 100 m for the 1990s, the modelling efficiency (MEF) (Stow et al., 2009) and logarithmic transformed root mean square error (RMSE) are indicated relative to observations from the WOA2009.